Accepted Manuscript

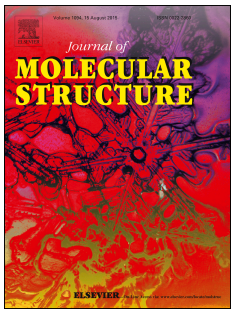

Studies on complex π-π and T-stacking features of imidazole and phenyl/*p*-halophenyl units in series of 5-amino-1-(phenyl/*p*-halophenyl)imidazole-4-carboxamides and their carbonitrile derivatives: Role of halogens in tuning of conformation

Aniruddha Das

PII: S0022-2860(17)30904-3

DOI: 10.1016/j.molstruc.2017.06.124

Reference: MOLSTR 24010

To appear in: *Journal of Molecular Structure*

Received Date: 17 May 2017

Revised Date: 25 June 2017

Accepted Date: 27 June 2017

Please cite this article as: A. Das, Studies on complex π-π and T-stacking features of imidazole and phenyl/*p*-halophenyl units in series of 5-amino-1-(phenyl/*p*-halophenyl)imidazole-4-carboxamides and their carbonitrile derivatives: Role of halogens in tuning of conformation, *Journal of Molecular Structure* (2017), doi: 10.1016/j.molstruc.2017.06.124.

Studies on complex π-π and T-stacking features of imidazole and phenyl/*p*-halophenyl units in series of 5-amino-1-(phenyl/*p*-halophenyl)imidazole-4-carboxamides and their carbonitrile derivatives: role of halogens in tuning of conformation

Aniruddha Das*

University College of Science, Technology & Agriculture,University of Calcutta, 92, Acharya Prafulla Chandra Road, Kolkata-700009

E-mail: aniruddha.1086@rediffmail.com Fax: + 91 033 2351 9755

Graphical Abstract

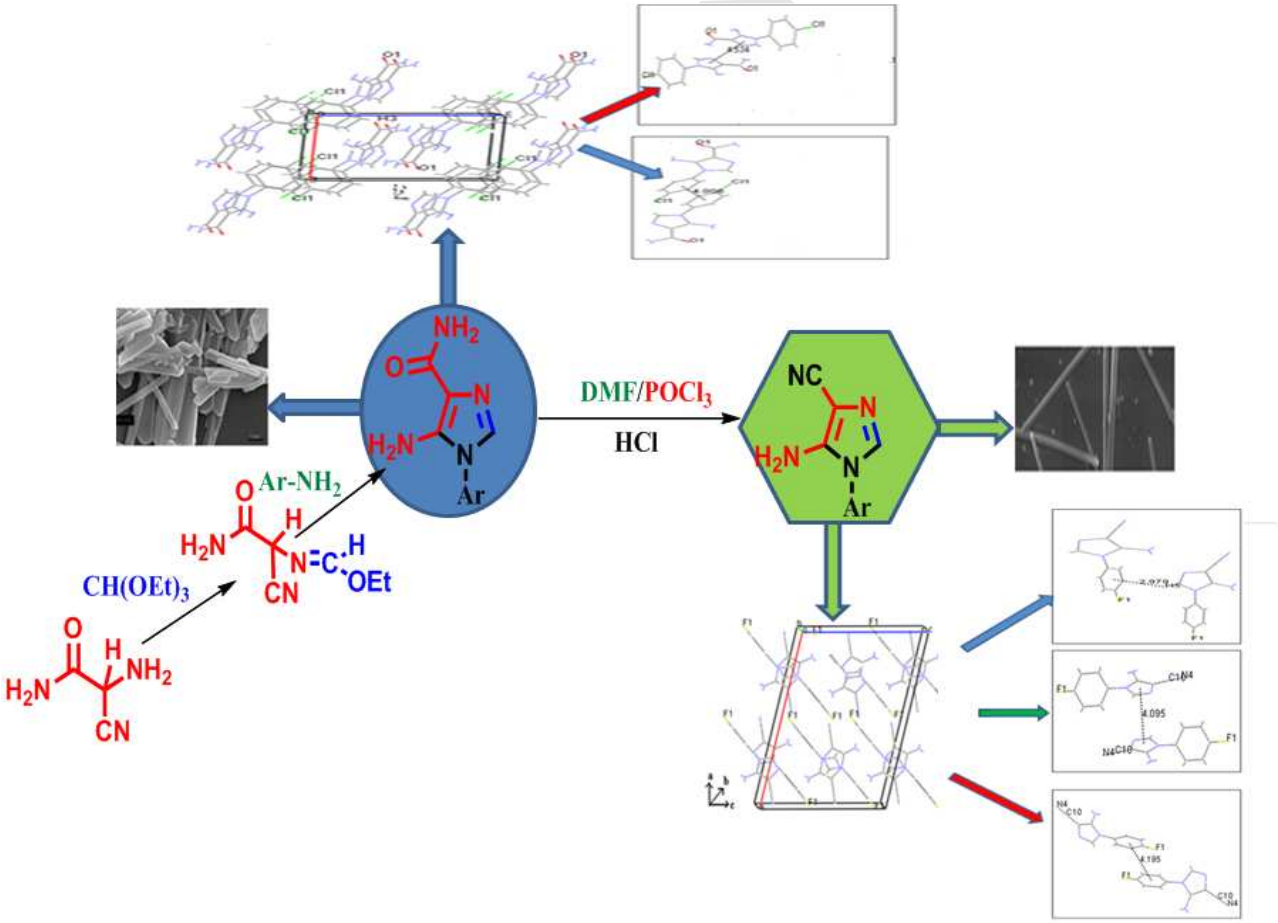

Studies on complex π-π and T-stacking features of imidazole and phenyl/*p*-halophenyl units in series of 5-amino-1-(phenyl/*p*-halophenyl)imidazole-4-carboxamides and their carbonitrile derivatives: role of halogens in tuning of conformation

Aniruddha Das*

University College of Science, Technology & Agriculture,University of Calcutta, 92, Acharya Prafulla Chandra Road, Kolkata-700009

E-mail: aniruddha.1086@rediffmail.com Fax: +91 033 2351 9755

Abstract

5-amino-1-(phenyl/*p*-halophenyl)imidazole-4-carboxamides (N-phenyl AICA) (**2a-e**) and 5-amino-1-(phenyl/*p*-halophenyl)imidazole-4-carbonitriles (N-phenyl AICN) (**3a-e**) had been synthesized. X-ray crystallographic studies of **2a-e** and **3a-e** had been performed to identify any distinct change in stacking patterns in their crystal lattice. Single crystal X-ray diffraction studies of **2a-e** revealed π-π stack formations with both imidazole and phenyl/*p*-halophenyl units in *anti* and *syn* parallel-displaced (PD)-type dispositions. No π-π stacking of imidazole occurred when the halogen substituent is bromo or iodo; π-π stacking in these cases occurred involving phenyl rings only. The presence of an additional T-stacking had been observed in crystal lattices of **3a-e**. Vertical π-π stacking distances in *anti*-parallel PD-type arrangements as well as T-stacking distances had shown stacking distances short enough to impart stabilization whereas *syn*-parallel stacking arrangements had got much larger π-π stacking distances to belie any *syn*-parallel stacking stabilization. DFT studies had been pursued for quantifying the π-π stacking and T-stacking stabilization. The plotted curves for *anti*-parallel and T-stacked moieties had similarities to the 'Morse potential energy curve for diatomic molecule'. The minima of the curves corresponded to the most stable stacking distances and related energy values indicated stacking

stabilization. Similar DFT studies on *syn*-parallel systems of **2b** corresponded to no π-π stacking stabilization at all. Halogen-halogen interactions had also been observed to stabilize the compounds **2d**, **2e** and **3d**. Nano-structural behaviour of the series of compounds **2a-e** and **3a-e** were thoroughly investigated.

Keywords

N-phenyl AICA; N-phenyl AICN; X-ray crystallography; C-H···π-stacking; DFT studies, self-aggregation.

1. Introduction

Intermolecular interactions are fundamentally important for predicting a gamut of phenomena ranging from simple acid-base behavior to functional nano-material formation [1-6]. In addition to hydrogen bonding interactions, π- π interactions [7], non-classical hydrogen bonds [8-10], halogen-halogen soft interactions [11-16] and non-covalent halogen bonds (X···N/O, X= halogens) [17-18] have been found to be instrumental, in various cases, in determining the physical and chemical properties of compounds with aromatic and heterocyclic rings and halogen substituents. Benzene-dimer serves as the prototypical model of π- π stacking and two most important structural minima for benzene dimers are the parallel-displaced (PD) π-stacked and C-H···π hydrogen bonded T-stacked structures [19-23]; parameterization of π- π stacking of benzene dimer have been the subject of many theoretical studies involving various functionals in the density functional theory (DFT). In case of parallel-stacked substituted benzene dimers, the aspects of the binding being stronger than the unsubstituted benzene, irrespective of the nature of substituents, have been reported; important contributions of dispersion, induction and exchange-repulsion items to the binding energy have also been considered [21,23,24]. Studies on π- π stacking of aromatically substituted N-heterocyclic molecules have gained momentum [25,26]. Imidazole is an acclaimed heterocyclic nucleus involved in various biochemical processes and pharmaceutics. AICA riboside (**1**) (Fig. 1) is the *de-nevo* purine precursor in the bio-synthetic pathway of purine nucleotides [27].

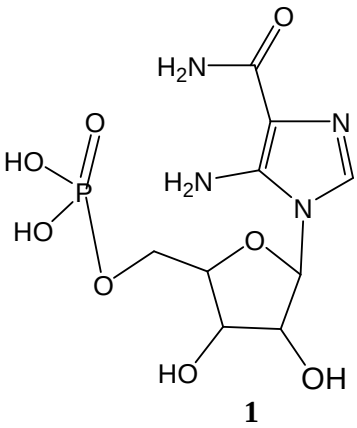

Fig. 1. Structure of AICAR (**1**)

In continuation of earlier work on AICA [28], recently I have reported [29] a systematic study on the π-π stacking features of a series 5-amino-1-alkylimidazole-4-carboxamides. This reports the fact that the imidazole units in these 1-alkylimidazole compounds show, in their X-ray crystallographic patterns, the very important *anti*-parallel and *syn*-parallel π-π stackings which were further supported by their DFT analysis. Since gas-phase benzene-dimer has reportedly got a binding energy of 2-3 Kcal mol^{-1}[30] I surmised to take up studies on similar AICA compounds where the imidazole unit holds a phenyl/*p*-halophenyl at N-1 instead of alkyl. The aspect of inclusion of an aryl substituent induced possible varieties of π-π stackings of homo-dimers (imidazole-imidazole and phenyl-phenyl) as well as hetero-dimer (imidazole-phenyl) types, along with the possible additional intricacies of the presence of *anti*-parallel and *syn*-parallel conformations. The conversion from 5-amino-1-(phenyl/*p*-halophenyl)imidazole-4-carboxamides (**2a-e**) to 5-amino-1-(phenyl/*p*-halophenyl)imidazole-4-carbonitriles (**3a-e**) was carried out to study the change in stack formation in the crystal lattice with the change of the functional group. DFT studies on these compounds had been pursued for the purpose of quantifying the stabilization in cases of π-π stacking of imidazole dimers and phenyl/*p*-halophenyl dimers as well as T-stacking interactions. In each case, DFT calculated results were in good agreements with the X-ray crystallographic

results. Recently there has been a surge of studies on π,π stacking-based organic materials to unravel unique optical and optoelectronic properties [31] being superior to the corresponding bulk counterparts. 1-D organic nanostructures have been successfully constructed by way of π- π stacking, hydrogen bonding [31,32] and electrostatic interactions, among others. Compounds **2a-c, 2e** and **3a-e** had shown to have generated 1-D nanostructures as well as **2d** had shown nano-vesicle morphology.

2. Experimental

2.1. Materials and methods

Melting points were recorded on an electrically heated Köfler Block apparatus and are uncorrected. The solid-state FT-IR measurements were done with a Perkin-Elmer-782 model spectrometer in the form of KBr discs of the compounds. ^{1}H NMR and ^{13}C NMR spectra were run with DMSO-d_6 solutions at ambient temperature on a Bruker Avance 300 spectrometer at 300 MHz for ^{1}H and at 75 MHz for ^{13}C. Chemical shifts are reported in δ and coupling constants in Hz. The multiplicity of the carbon atoms was determined by the DEPT 135º experiment**.** The DFT calculations had been performed by using the basis set mpwb95/6-31++g for **2a-d** and **3a-d** as well as mpwb95/lanl2dz for **2e** and **3e** in **Gaussian 09W** [33] suite of programs. These basis sets included correlation consistent methods which consist of diffusion correction being advantageous for our targets of π-π stacking calculation considered upto long range.

2.2. General procedure for the preparation of 5-amino-1-(phenyl/p-halophenyl) imidazole-4-carboxamides **(2a-e)**

Syntheses of compounds **2a** and **2c** were reported [34]. The same protocol was utilized to synthesize three new compounds **2b**, **2d** and **2e** of the series of **2a-e**.

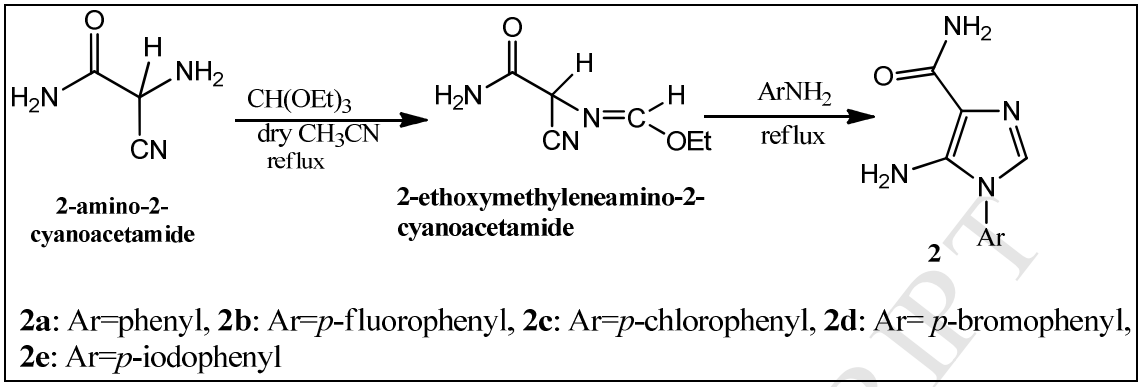

2a: Ar=phenyl, **2b**: Ar=*p*-fluorophenyl, **2c**: Ar=*p*-chlorophenyl, **2d**: Ar= *p*-bromophenyl, **2e**: Ar=*p*-iodophenyl

Scheme 1. Preparation of 5-amino-1-(phenyl/*p*-halophenyl)imidazole-4-carboxamide compounds (**2a-e**)

To freshly prepared 2-amino-2-cyanoacetamide (0.02mol) in dry and freshly distilled acetonitrile (15 ml) triethyl orthoformate (0.02 mol) was added and the mixture was heated under reflux for 40 minutes. To the reaction mixture at room temperature aniline/ *p*-haloaniline (0.02 moles) was then added. The reaction mixture was refluxed for 30 min. when the title compound began to precipitate. The reaction mixture was allowed to cool. The ice-cooled mixture was filtered and washed with a little of acetonitrile. The crude product was crystallized from aqueous ethanol.

*2.2.1. 5-Amino-1-phenylimidazole-4-carboxamide (**2a**)*

Colourless crystal (from aq. EtOH), yield 59.4%, m.p. 202 °C: ^{1}H NMR (300 Mhz, DMSO-d$_6$): δ_H 7.37 (1H, s, 2-*H*), 5.76 (2H, s, O=*C*-N*H*$_2$), 6.81 & 6.96 (2H, pair of br. s, -N*H*$_2$), 7.52 (5H, m, *o*, *m* and *p*-protons); ^{13}C NMR (75MHz, DMSO-d$_6$): δ_C 128.57 (2-*C*), 113.48 (4- *C*), 143.09 (5-*C*) , 167.21 (O=*C*-NH$_2$), 135.09 (1′-*C*), 125.00 (2′-*C* & 6′-*C*), 130.28 (3′-*C* & 5′-*C*), 130.14 (4′-*C*) ; IR υ_{max}(KBr), cm^{-1}: 3750 (amide N-H), 3396 (amino N-H), 3189 (aromatic C-H), 1667 (amide –C=O), 1548 (aromatic C=C).

2.2.2. 5-Amino-1-(4-fluorophenyl)imidazole-4-carboxamide (**2b**)

Colourless crystal (from aq. EtOH), yield 63.63%, m.p. 282-284°C: δ_H 7.30 (1H, s, 2-*H*), 5.71 (2H, s O=C-NH_2), 6.75 & 6.90 (2H, pair of br. s, -NH_2), 7.36 (2H, t, J 8.7 Hz, 2′-*H* & 6′-*H*), 7.50 (2H, m, 3′-*H* & 5′-*H*), ^{13}C NMR (75MHz, DMSO-d_6): δ_C 129. 86 (2-*C*), 112.96 (4-*C*), 142.88 (5-*C*) , 166.80 (O=*C*-NH_2), 131.02 (1′-*C*), 127.28 (dd, $^3J_{C-F}$ 9.0 Hz , 2 ′-*C* & 6 ′-*C*), 116.68 (dd, $^2J_{C-F}$ 23.25 Hz , 3 ′-*C* & 5 ′-*C*), 161.59 (d, $^1J_{C-F}$ 244.5 Hz ,4′-*C*); IR υ_{max}(KBr), cm^{-1}: 3770 (amide N-H), 3331.5 (amino N-H), 3110 (aromatic C-H), 1666 (amide –C=O), 1556 (aromatic C=C).

*2.2.3. 5-Amino-1-(4-chlorophenyl)imidazole-4-carboxamide (**2c**)*

Colourless crystal (from aq. EtOH), yield 67.68%, m.p. 258-260°C: ^{1}H NMR (300 Mhz, DMSO-d_6): δ_H 7.38(1H, s, 2-*H*), 5.81 (2H, br.*s*, O=C-NH_2), 6.82 and 6.97 (2H, pair of br. s., -NH_2), 7.54 (2H, d, J 8.7 Hz, 2′-*H* & 6′-*H*), 7.63 (2H,d, J 8.7 Hz, 3′-*H* & 5′-*H*), ^{13}C NMR (75MHz, DMSO-d_6): δ_C 130.04 (2-*C*), 113.49 (4-*C*), 143.08 (5-*C*) , 167.13 (O=*C*-NH_2), 133.96 (1′-*C*), 126.95 (2′-*C* & 6′-*C*), 130.18 (3′-*C* & 5′-*C*), 133.08 (4′-*C*) ; IR υ_{max}(KBr), cm^{-1}: 3755 (amide N-H), 3322 (amino N-H), 3103 (aromatic C-H), 1666 (amide –C=O), 1552 (aromatic C=C).

*2.2.4. 5-Amino-1-(4-bromophenyl)imidazole-4-carboxamide (**2d**)*

Colourless crystal (from aq. EtOH), yield 64.05%, m.p. 254-256°C: ^{1}H NMR (300 Mhz, DMSO-d_6): δ_H 7.34 (1H, s, 2-*H*), 5.78 (2H, br.*s*, O=C-NH_2), 6.78 & 6.94 (2H, pair of br. s ,-NH_2), 7.71 (2H, d, J 8.6 Hz, 2′-*H* & 6′-*H*), 7.43 (2H, d, J 8.6 Hz, 3′-*H* & 5′-*H*), ^{13}C NMR (75MHz, DMSO-d_6): δ_C 129.63 (2-*C*), 113.11 (4- *C*), 142.68 (5-*C*) , 166.76 (O=*C*-NH_2), 134.00 (1′-*C*), 126.86 (2′-*C* & 6′-*C*), 132.77 (3′-*C* & 5′-*C*), 121.11 (4′-*C*) ; IR υ_{max}(KBr), cm^{-1}: 3763 (amide N-H), 3332 (amino N-H), 3169 (aromatic C-H), 1655 (amide –C=O), 1540 (aromatic C=C).

*2.2.5. 5-Amino-1-(4-iodophenyl)imidazole-4-carboxamide (**2e**)*

Colourless crystal (from aq. EtOH), yield 61.19%, m.p. 270-272°C: ^{1}H NMR (300 Mhz, DMSO-d_6): δ_H 7.32(1H, s, 2-*H*), 5.76 (2H, br.*s*, O=C-NH_2), 6.75 & 6.93 (2H, pair of br. s ,-NH_2), 7.27 (2H, d, J 8.4 Hz, 2′-*H* & 6′-*H*), 7.86 (2H, d, J 8.4 Hz, 3′-*H* & 5′-*H*), ^{13}C NMR (75MHz, DMSO-d_6): δ_C 129.73 (2-*C*), 113.05 (4-*C*), 142.75 (5-*C*) , 166.86 (O=*C*-NH_2), 134.45 (1′-*C*), 126.95 (2′-*C* & 6′-*C*), 138.75 (3′-*C* & 5′-*C*), 94.10 (4′-*C*) ; IR υ_{max}(KBr), cm^{-1}: 3763 (amide N-H), 3319 (amino N-H), 3188 (aromatic C-H), 1651 (amide –C=O), 1529 (aromatic C=C) .

*2.3. General procedure for the preparation of 5-amino-1-(phenyl/p-halophenyl)imidazole-4-carbonitrils (**3a-e**)*

Synthesis of compound **3c** was reported in literature. Four new compounds **3a-b** and **3d-e** of the series of **3a-e** are reported in this paper.

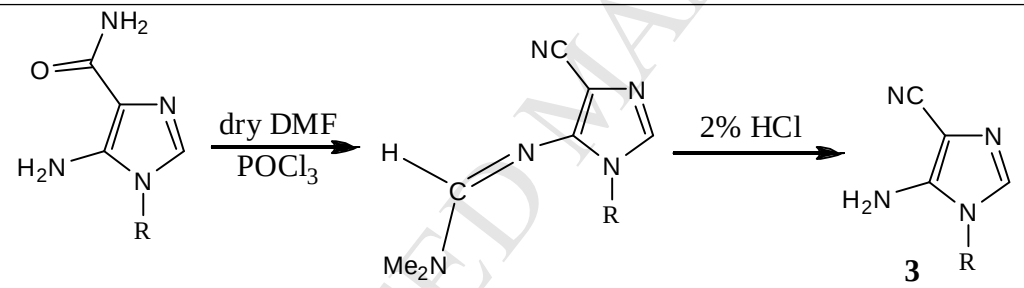

3a: R= phenyl, **3b**: R= *p*-fluorophenyl , **3c**: R= *p*-chlorophenyl, **3d**: R= *p*-bromophenyl, **3e**: R= *p*-iodophenyl

Scheme 2. Preparation of 5-amino-1-(phenyl/*p*-halophenyl)imidazole-4-carbonitrile compounds (**3a-e**)

5-amino-1-(phenyl/*p*-halophenyl)imidazole-4-carboxamides (**2**) (4mmol) was added in portions to ice-cold dimethylformamide-phosphorous oxychloride complex, prepared from DMF (6ml) and $POCl_3$ (1.2 ml, 12 mmoles), during 15 min with stirring. After the addition was complete, the mixture was kept in the ice bath for 30 min. Then the mixture was allowed to warm up to room temperature and kept at room temperature for a further period of 90 min, stirring being continued all the time. The resulting wine red

solution was poured into crushed ice. The solution was made strongly ammoniacal. A brown solid was precipitated. Then it was filtered and the brown mass was warmed on a steam bath with 2% aq. hydrochloric acid (50 ml) for 1 hour. Afterthat, it was allowed to cool in ice-bath and made strongly ammoniacal. The solid was precipitated and ice-cooled mixture was then filtered. The crude product was crystallized from aqueous ethanol.

*2.3.1. 5-Amino-1-phenylimidazole-4-carbonitrile (**3a**)*

Colourless crystal (from aq. EtOH), yield 54.94%, m.p. 182-184 °C: ^{1}H NMR (300 Mhz, DMSO-d_6): δ_H 7.41 (1H, s, 2-*H*), 6.15 (2H, s,-NH_2), 7.45-7.60 (5H, m, *o*, *m* and *p*-protons); ^{13}C NMR (75MHz, DMSO-d_6): δ_C 133.07 (2-*C*), 91.67 (4-*C*), 147.70 (5-*C*) , 117.50 (-*C*N), 134.38 (1′-*C*), 125.77 (2′-*C* & 6′-*C*), 130.34 (3′-*C* & 5′-*C*), 129.17 (4′-*C*); IR(KBr, cm^{-1}): 3317 (amino N-H), 3175 (aromatic C-H), 2211(-C≡N), 1578 (aromatic C=C).

*2.3.2. 5-Amino-1-(4-fluorophenyl)imidazole-4-carbonitrile (**3b**)*

Colourless crystal (from aq. EtOH), yield 60.10%, m.p. 198-200 °C: ^{1}H NMR (300 Mhz, DMSO-d_6): δ_H 7.45-7.50 (2H, m, 2′-*H* &6′-*H*), 7.33-7.38 (3H, m, 2-*H*, 3′-*H* & 5′-*H*), 6.12 (2H, s, -NH_2); ^{13}C NMR (75MHz, DMSO-d_6): δ_C 133.09 (2-*C*), 91.39 (4-*C*), 147.96 (5-*C*), 117.47 (-*C*N), 130.64 (1′-*C*, $^{4}J_{C-F}$ 3 Hz), 128.5 (2′-*C* & 6′-*C*, $^{3}J_{C-F}$ 9 Hz), 117.11 (3′-*C* & 5′-*C*, $^{2}J_{C-F}$ 23.25 Hz), 162.31 (4′-*C*, $^{1}J_{C-F}$ 243.75 Hz).; IR υ_{max}(KBr), cm^{-1}: 3339.4 (amino N-H), 3191(aromatic C-H), 2368.9, 2217 (-C≡N), 1582 (aromatic C=C).

*2.3.3. 5-Amino-1-(4-chlorophenyl)imidazole-4-carbonitrile (**3c**)*

Colourless crystal (from aq. EtOH), yield 55.55%, m.p. 196-198°C: ^{1}H NMR (300 Mhz, DMSO-d_6): δ_H 7.35 (1H, s, 2-*H*), 6.16 (2H, s,-NH_2), 7.44 (2H, d, J 2.1 Hz, J 6.6 Hz, 2′-*H* &6′-*H*), 7.57 (2H, d, J 2.1 Hz, J 6.6 Hz, 3′-*H* & 5′-*H*); ^{13}C NMR (75MHz, DMSO-d_6): δ_C 132.67 (2-*C*), 91.26 (4-*C*) , 147.52 (5-*C*) , 117.11 (-*C*N), 133.55 (1′-*C*), 127.55 (2′-*C* & 6′-*C*), 130.00 (3′-*C* & 5′-*C*), 132.88 (4′-*C*); IR υ_{max}(KBr), cm^{-1}: 3324 (amino N-H), 3175 (aromatic C-H), 2213 (-C≡N), 1577 (aromatic C=C).

*2.3.4. 5-Amino-1-(4-bromophenyl)imidazole-4-carbonitrile (**3d**)*

Colourless crystal (from aq. EtOH), yield 58.82%, m.p. 202-204°C: ^{1}H NMR (300 Mhz, DMSO-d_6): δ_H 7.37 (1H, s, 2-*H*), 6.19 (2H, s,-NH_2), 7.39 (2H, d, J 7.8 Hz, 2′-*H* &6′-*H*), 7.71 (2H, d, J 7.8 Hz, 3′-*H* &5′-*H*); ^{13}C NMR (75MHz, DMSO-d_6): δ_C 132.47 (2-*C*), 91.19 (4-*C*), 147.36 (5-*C*) , 117.03 (-*C*N), 133.26 (1′-*C*), 127.68 (2′-*C* & 6′-*C*), 132.81 (3′-*C* & 5′-*C*), 121.85 (4′-*C*); IR υ_{max}(KBr), cm^{-1}: 3317 (amino N-H), 3183 (aromatic C-H), 2207 (-C≡N), 1568 (aromatic C=C).

*2.3.5. 5-Amino-1-(4-iodophenyl)imidazole-4-carbonitrile (**3e**)*

Colourless crystal (from aq. EtOH), yield 53.19%, m.p. 238-240 °C: ^{1}H NMR (300 Mhz, DMSO-d_6): δ_H 7.40 (1H, s, 2-*H*), 6.21 (2H, s, -NH_2), 7.28 (2H, d, J 8.4 Hz, 2′-*H* & 6′-*H*), 7.91 (2H, d, J 8.4 Hz, 3′-*H* & 5′-*H*); ^{13}C NMR (75MHz, DMSO-d_6): δ_C 132.83 (2- *C*), 91.64 (4-*C*) , 147.67 (5-*C*) , 117.42 (-*C*N), 134.11 (1′-*C*), 128.02 (2′-*C* & 6′-*C*), 139.06 (3′-*C* & 5′-*C*), 95.28 (4′-*C*); IR υ_{max}(KBr), cm^{-1}: 3314 (amino N-H), 3184 (aromatic C-H), 2205 (-C≡N), 1517.3 (aromatic C=C).

2.4. Determination of crystal structure

For the purpose of single crystal X-ray diffraction studies, triple distilled ethanol properly diluted with double distilled water to get aqueous ethanol was used as solvent of crystallization; suitable single crystals of compounds **2a-e** and **3a-e** were obtained by recrystallization of the material from this freshly prepared aqueous ethanol. Diffraction data were collected for **2a-e** and **3a-e** using the freshly crystallized material with MoKα radiation at 296 K using a Bruker APEX-II CCD system. The crystals were positioned 50 mm from the CCD. Frames were measured with a counting time of 10 s. During collection of data none of **2a-e** and **3a-e** showed any evidence of crystal decay. Data analyses were carried out with the Bruker APEX2 and Bruker SAINT programs. The structures were solved using direct methods with the SHELXTL 97 program (Sheldrick, 2008).

The ORTEP diagram of representative compound 5-amino-1-(4-bromophenyl)imidazole-4-carboxamide (**2e**) of the series **2a-e** and 5-amino-1-(4-iodophenyl)imidazole-4-carbonitrile (**3d**) of the series **3a-e** are shown in Fig. 2 and Fig. 3 respectively.

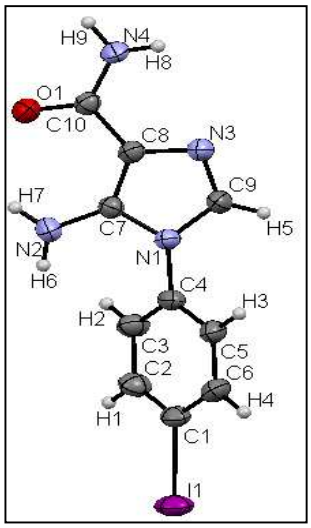

Fig. 2. ORTEP diagram of compound **2e**
CCDC no. **1050706**

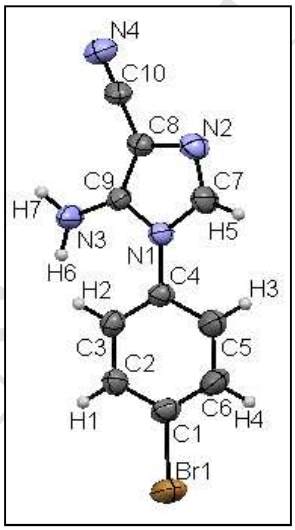

Fig. 3. ORTEP diagram of compound **3d**
CCDC no. **1050710**

3. Results and discussion

3.1. Description of crystal structure

The observations that X-ray crystallographic analyses have been successful in unraveling stacked arrangements in case of drug molecules and in the aromatic side-chains of proteins [36, 37] have infused interest in the prediction of the role of stacking interaction on the stabilization of supramolecular architecture. These findings have generated motivation for knowing its role in quantitative structure-activity relationships [38]. The self-assembled supramolecular structure formation is intrigued in many cases by π-π stacking as an important non-covalent force. As early as in 1938, Astbury and Bell [39] reported a spacing of 3.3-3.4 Å between flat or almost flat nucleotide units existing perpendicular to the long axis of the molecules. Studies on aromatic stacking interactions using conformationally flexible

molecules have been the focus of a no. of relevant experiments [40]. Although there have been some experimental and DFT studies on the π-π-stacking of several systems containing N-heterocyclic units, a recent report [29] of studies on π-π stacked imidazole systems have unraveled, for the first time, the role of π-π stacking of imidazoles in the *anti*-parallel conformations as the stabilizing factor in the crystal lattice of a series of 5-amino-1-alkylimidazole-4-carboxamides; corresponding *syn*-parallel conformation failed to tender any appreciable stabilization. I describe here in a systematic way the synthesis of series of compounds **2a-e** and **3a-e** where the *halo* moiety embraces all the possible choices out of F, Cl, Br, I. It was expected that the halogens with the widely varying electronegativities and sizes would sometime offer drastically different situations. DFT studies had also been taken up in a cue. Parallel-displaced (PD) [41] π-π stack formations had been observed in the X-ray crystallographic studies for **2a-e**, occurring with both imidazole and phenyl/*p*-halophenyl units in mutually *anti*-parallel and *syn*-parallel arrangements. The crystal lattices of **3a-e** revealed the presence of T-stackings along with the PD-stacked *anti*-/*syn*-parallel π-π stackings of both imidazole-imidazole and phenyl-phenyl/*p*-halophenyl-*p*-halophenyl rings of two correspondingly adjacent AICA derivatives. The crystal lattices of **2a-e** did not show any T-stacking. No hetero-dimer formation was noted in the crystal lattice of **2a-e** and **3a-e**. In cases of **2d-e** and **3a-e** some different behaviours were observed.

Table 1 contains the details of crystal data showing the bond lengths and angles of **2a-e** and Table 2 tabulates the similar data of **3a-e**.

Table 1
Crystal data of **2a-e**

Compound	**2a**	**2b**	**2c**	**2d**	**2e**
Formula	$C_{10}H_{10}N_4O_1$	$C_{10}H_9F_1N_4O_1$	$C_{10}H_9Cl_1N_4O_1$	$C_{10}H_9Br_1N_4O_1$	$C_{10}H_9I_1N_4O_1$
M/g mol^{-1}	202.22	220.21	236.66	281.12	328.11
Crystal system	triclinic	triclinic	triclinic	monoclinic	monoclinic

Space group	P-1	P-1	P-1	C12/c1	C12/c1
a (Å)	7.6252(7)	7.6579(12)	7.723(8)	20.193(5)	13.667(3)
b (Å)	7.9439(7)	7.7666(14)	8.005(8)	10.467(2)	10.732(2)
c (Å)	9.0756(9)	9.1625(14)	9.366(10)	14.481(3)	15.228(3)
α (°)	86.642(5)	87.927(8)	85.799(13)	90.00	90.00
β (°)	87.258(4)	88.210(8)	89.218(13)	134.166(11)	90.462(8)
γ (°)	62.767(4)	63.477(7)	63.289(12)	90.00	90.00
V (A^{o3})	487.83(8)	487.21(14)	515.7(9)	2195.5(8)	2233.5(8)
Z	2	2	2	8	8
ρ_C / g cm $^{-3}$	1.377	1.501	1.524	1.701	1.952
Absorption μ / mm-1	0.095	0.116	0.353	3.728	2.852
Min. T	0.9720	0.9660	0.9016	0.3553	0.4817
Final R indices [I>2σ(l)] R_1	0.0533	0.0405	0.0519	0.0380	0.0341
wR_2	0.1561	0.1209	0.1394	0.1060	0.0826
R indices (all data) R_1	0.0621	0.0470	0.0915	0.0528	0.0522
wR_2	0.1707	0.1364	0.1743	0.1190	0.0930
Recrys. from	hot aq. ethanol	hot aq. ethanol	hot aq. ethanol	hot aq. ethanol	hot aq. Ethanol
CCDC number	1050702	1050703	1050704	1050705	1050706

Table 2
Crystal data of **3a-e**

Compound	**3a**	**3b**	**3c**	**3d**	**3e**
Formula	$C_{10}H_8N_4$	$C_{10}H_7F_1N_4$	$C_{10}H_7Cl_1N_4$	$C_{10}H_7Br_1N_4$	$C_{10}H_7I_1N_4$
M/g mol^{-1}	184.20	202.20	218.65	263.11	310.10

Crystal system	triclinic	monoclinic	monoclinic	monoclinic	monoclinic
Space group	P-1	C12/c1	P121/c1	P121/c1	P121/c1
a (A°)	6.2970(12)	18.045(5)	18.571(3)	11.1107(7)	10.947(3)
b (A°)	9.248(2)	8.967(2)	18.342(3)	6.4150(4)	6.4268(14)
c (A°)	17.470(3)	12.304(3)	12.0976(17)	15.0571(9)	15.673(4)
α (°)	92.896(10)	90.00	90.00	90.00	90.00
β (°)	91.266(9)	103.385(3)	99.784(2)	105.805(2)	105.432(9)
γ (°)	107.490(10)	90.00	90.00	90.00	90.00
V ($A°^3$)	968.4(3)	1936.9(9)	4060.9(10)	1032.62(11)	1062.9(4)
Z	4	8	16	4	4
ρ_C / g cm^{-3}	1.263	1.387	1.430	1.692	1.938
Absorption μ / mm^{-1}	0.082	0.103	0.345	3.950	2.983
Correctiontype Max. T	0.9919	0.9898	0.9684	0.6486	0.7546
Min. T	0.9758	0.9698	0.9092	0.3646	0.4681
Final Rindices [I>2σ(l)] R_1	0.0490	0.0471	0.0440	0.0364	0.0276
wR_2	0.1562	0.1367	0.1328	0.0952	0.0660
R indices (all data)R_1	0.0671	0.0893	0.0955	0.0508	0.0398
wR_2	0.1843	0.1747	0.1841	0.1055	0.0722
Recrys.from	hot aq. ethanol	hot aq. ethanol	hot aq. ethanol	hot aq. ethanol	hot aq. ethanol
CCDC number	1050707	1050708	1050709	1050710	1050711

The extensive H-bonding patterns of representative compounds **2d** of the series **2a-e** and **3a** of the series **3a-e** are shown in Fig. 4. The hydrogen bonding patterns are presented in Supplementary data**,** Fig. S21

and Fig. S22 as well as the hydrogen bonding parameters for the compounds **2a-e** and **3a-e** are presented in Supplementary data**,** Table S2 and Table S3.

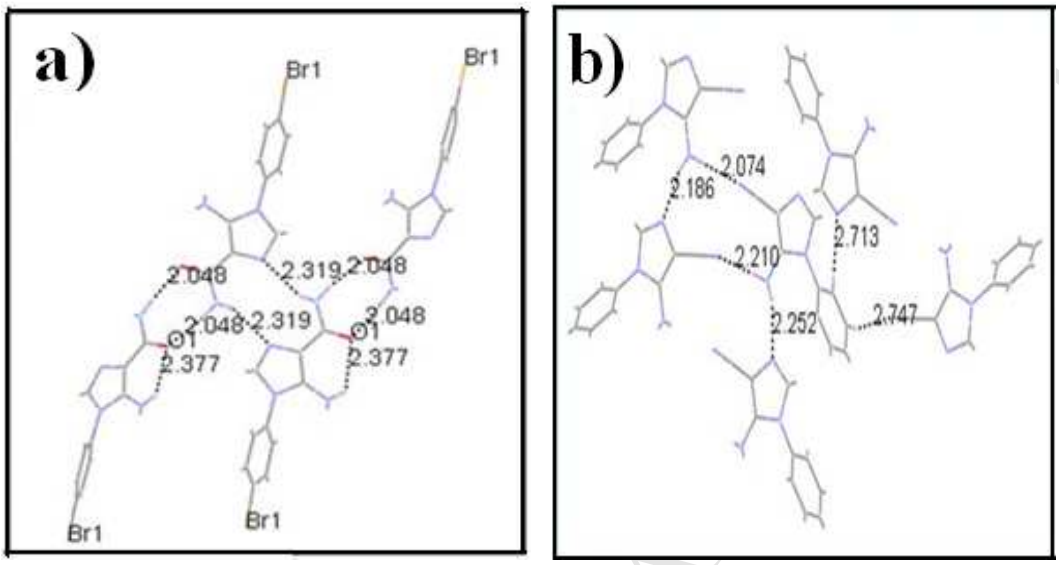

Fig. 4. a) and b) show hydrogen bonding network of **2d** and **3a** respectively

The unit cell arrangement of the lattice of representative compound **2c** is shown in Fig. 5a. Fig. 5b and Fig. 5c reveal the features of π-π stacking of imidazole-imidazole and *p*-chlorophenyl-*p*-chlorophenyl units respectively in PD-type *anti*-parallel arrangements.

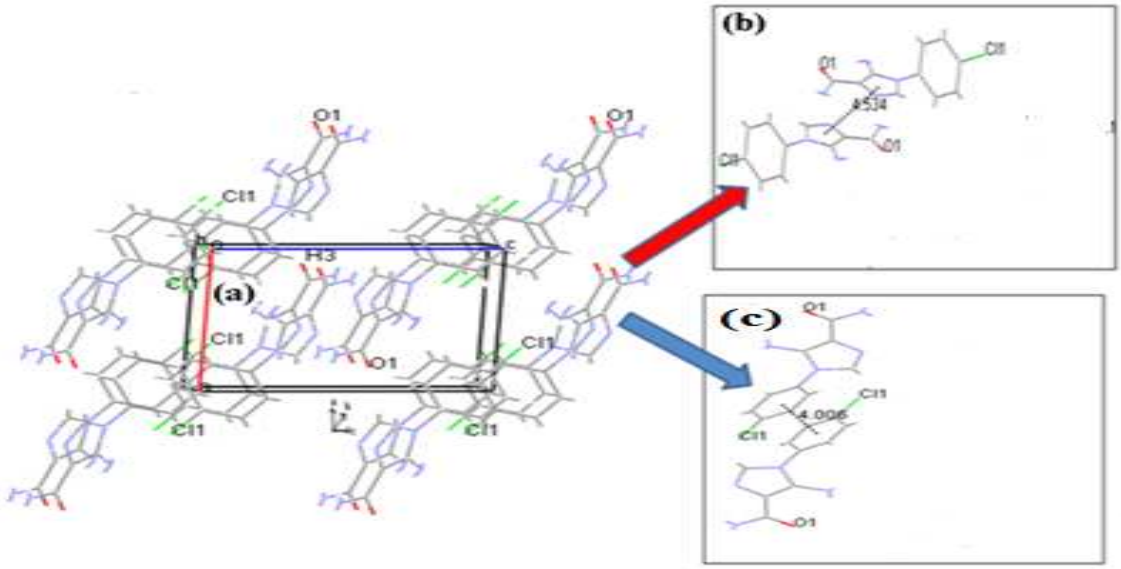

Fig. 5. (a) unit cell arrangement viewing along b-direction, (b) π- π stacking of two *anti*-parallel imidazoles observed in X-ray crystallographic lattice and (c) π- π stacking of two *anti*-parallel phenyls observed in X-ray crystallographic lattice of compound **2c**.

Similar *anti*-parallel PD-stacked imidazole-imidazole and phenyl-phenyl π-π stacking interactions were observed in the crystal lattices of **2a** and **2b** (shown in Supplementary data, Fig. S54 and Fig. S55 respectively) where the N1 substituents of AICA were phenyl and *p*-fluorophenyl groups respectively. It was further observed from the X-ray studies of **2d** and **2e,** where the halogen substituents were of larger size viz. *p*-bromophenyl- and *p*-iodophenyl- as the N-1 substituents respectively, the closely-associated imidazole rings were not oriented in *anti*-parallel fashion. The closest imidazole rings in the corresponding crystal lattices displayed dihedral angels of 65.49˚ and 70.41˚ respectively (shown in Fig. 6a. and Fig. 6b.). These large dihedral angles of closely-associated imidazole rings of **2d** and **2e** exerted difficulty for imidazole-imidazole *anti*-parallel π-π stacking.

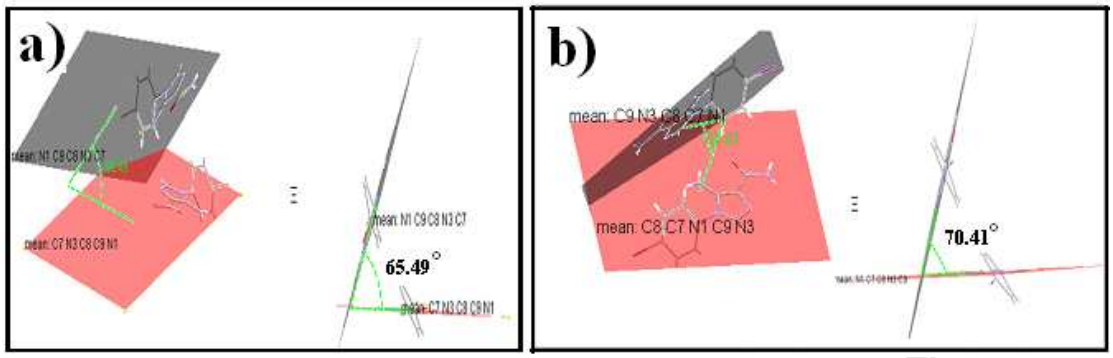

Fig. 6. a) and b) show Dihedral angle between the closest pair of imidazoles in the lattice of **2d** and **2e** respectively

Table 3 presents the *anti*-parallel PD π-π stacking distances between imidazole-imidazole of compounds **2a-c** and similar π-π stacking distances between phenyl-phenyl moieties of **2a-c** and **2e** with their respective slip angle values. The respective vertical distance values for those compounds are tabulated in Table 3**.** Another important parameter termed as "vertical distance" [42] is defined as the shortest distance between two stacked molecules and is represented by R_2 (Fig. 7). The value of R_2 could be calculated from the Equation 1 where R_1 is the distances observed between π-π stacked parallel-displaced imidazoles and θ is designated as slip angle. The slip angle is essentially the angular deviation from the PD-stacked imidazoles and hypothetical sandwich-stacked imidazoles.

$$R_2=R_1 \cos\theta \quad \text{.....Equation 1}$$

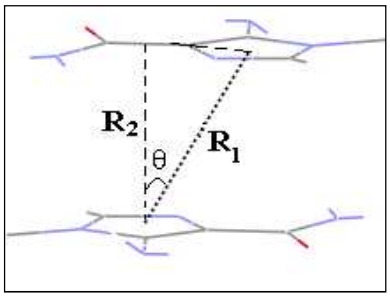

Fig. 7. The vertical distance (R_2), PD-stacked imidazole-imidazole distance (R_1) and slip angle (θ)

Similarly, measurements of slip angle and vertical distances between PD-stacked phenyl/*p*-halophenyls of compounds **2a-e** were calculated (shown in Supplementary data**,** Fig.S24- Fig.S42)**.** Table 3 shows distances between centroids of two imidazoles and centroids of two phenyls in *anti*-parallel stacking arrangements were in the range of 4.43-4.53 and 4.01-4.46 Å respectively. These were the experimental *anti*-parallel PD π-π stacking distances. In each case of a PD-stacked dimer, the corresponding vertical distance of *anti*-parallel imidazole dimer as well as that of the phenyl/*p*-halophenyl dimer are shown in Table 3**.** The vertical distances in the case of phenyl dimers were in the range of 3.83-4.07 Å and those in the case of imidazole dimers lie in the range of 4.20-4.36 Å (Table 3). Although each of the crystal lattice of **2a**, **2b**, **2c** and **2e** corresponded to *anti*-parallel conformation of the phenyl/*p*-halophenyl moieties in PD-type arrangements[41], compound **2d** had got a sensibly sandwich-type *anti*-parallel stacking of *p*-bromophenyl moiety. The π-π stacking distance can very often be considered as a marker of the strength of stacking interaction. With the results of *Ab-initio* calculation, Sinnokort *et.al.* [30] have ascertained a value of 3.4 Å for vertical separation between the planes of PD π-π stacked benzenes. The earlier report [29] of the vertical distances of *anti*-parallel imidazole dimers of 5-amino-1-alkylimidazole-4-carboxamides, lying in the range 3.70-3.89 Å, can be compared with π-π *anti*-parallel stacking stabilization.

Table 3

Anti-parallel PD π-π stacking distances from X-ray crystallographic analysis of **2a-e** and the corresponding vertical π-π stacking distances

Compound	*imidazole-imidazole* *anti*-parallel π-π stacking			Phenyl/*p*-halophenyl-phenyl/*p*-halophenyl *anti*-parallel π-π stacking		
	π-π stacking distance from crystal lattice (Å)	slip angle from crystal lattice (º)	vertical π-π distance (Å)	π-π stacking distance from crystal lattice(Å)	slip angle from crystal lattice(º)	vertical π-π distance (Å)

2a	4.53	16.08	4.35	4.14	15.19	3.99
2b	4.43	18.30	4.20	4.46	30.88	3.83
2c	4.53	15.63	4.36	4.01	6.49	3.98
2d	-	-	-	**4.04**[#]	-	-
2e	-	-	-	4.20	14.15	4.07

PD π-π stacking distance between *p*-bromophenyls for **1d** is essentially "Sandwich" stacking

A comparison of vertical *anti*-parallel phenyl-phenyl stacking distances (Table 3) also revealed that vertical distance for fluoro compound (**2b**) is the least (3.83 Å) and this value increased steadily in going from fluoro to iodo in the series of **2b-2e**. Among all the halogens, fluorine with the highest electronegativity value of 4.0, a negative inductive effect value (σ_I) of 0.51 and a positive mesomeric effect (σ_R) of -0.34 can show strong intramolecular interactions in case of organic fluoro compounds [43]. In 2000, Prasanna and Guru Row [44] have published a data base study on the influence of C-F…π interactions on crystal packing and conformations. Recently S.Terada *et.al.* [45] have published an account of polymorphism of different fluoro-substituted aromatic sulfonamides showing dependence on intermolecular π-π interactions. Sinnokrot *et. al.* [24] have earlier communicated DFT studies on the effect of substituent of a substituted-benzene unit on the binding with an unsubstituted benzene where –F and -CN substituents correspond to much higher binding energies and lower distances between the centroids of the rings. It had been discussed earlier that the *anti*-parallel PD π-π stackings between imidazole-imidazole pairs were not feasible in cases of **2d-e.** The phenyl-phenyl stacking for the compound **2d** was actually "Sandwich" (S) in nature which was evidenced from Fig. 8b. *Anti*-parallel PD-stacked *p*-iodophenyl-*p*-iodophenyl π-π stacking interaction of compound **2e** is shown in Supplementary data, Fig.S56.

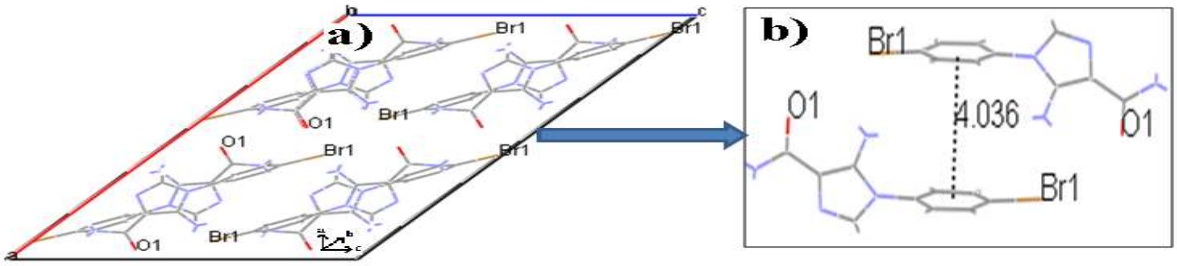

Fig. 8. (a) unit cell arrangement viewing along b-direction of **2d**, (b) sandwich type π-π stacking of two *anti*-parallel *p*-bromophenyls

Literature survey revealed that PD-type π-π stacking was generally more stabilizing in nature than the S-type [30]. Overall stabilization of the lattices of **2d** and **2e** must have come from a balance of other stabilizing features e.g. halogen-halogen soft interactions etc. Simultaneously, we could take out the closest *syn*-parallel dimer in the same fashion to get the π-π stacking distances between the centroids of the two imidazole units and the centroids of the two phenyl units to have the identical values, irrespective of slightly different slip angle [42]. They lie in the range of 7.66-11.63 Å. Table 4 shows the *syn*-parallel π-π stacking distances between imidazole-imidazole and phenyl-phenyl stacked moieties obtained from X-ray crystallographic analysis for the compounds **2a-e**. Due to variation in the slip angles between the π-π stacked imidazole-imidazole and phenyl-phenyl moieties, differences in vertical distances for those pairs were observed.

Table 4
Syn-parallel π-π stacking distances from X-ray crystallographic analysis of **2a-e** and the corresponding vertical π-π stacking distances

Compound	*imidazole-imidazole* *anti*-parallel π-π stacking			Phenyl/*p*-halophenyl-phenyl/*p*-halophenyl *anti*-parallel π-π stacking		
	π-π stacking distance from crystal lattice (Å)	slip angle from crystal lattice (°)	vertical π-π distance (Å)	π-π stacking distance from crystal lattice(Å)	slip angle from crystal lattice(°)	vertical π-π distance (Å)

2a	7.94	30.91	6.81	7.94	25.45	7.17
2b	7.66	21.07	7.14	7.66	26.20	6.87
2c	8.25	55.24	4.70	8.25	54.69	4.77
2d	11.63	17.62	11.08	11.63	19.31	10.97
2e	8.69	12.79	8.47	8.69	13.63	8.44

It was interesting to note that, for compounds **2a-e**, the phenyl/*p*-halophenyl units are attached to respective N-1 of imidazole units with a free-rotable single bond. The lattices showed that the values of torsion angles between the imidazole and the respective N1 phenyl/*p*-halophenyl ring for those AICA derivatives were in the range of │43.75°│ to │52.16° │(please see Supplementary data, Table S4). As a consequence, mixed imidazole-phenyl stacking was not possible in crystal lattices of **2a-e**. Occurrences of preferential intramolecular π-π stabilizing interactions between two aromatic components of a sufficiently flexible molecule is documented [46-50]. These molecules are known as foldamers [51]. This phenomenon can be related to the optimized conformation of a molecule in its crystalline lattices maintaining a balance of size, electronegativity and electronaffinity of the halogens/substituents (please see Supplementary data, Table S1). None of the molecules **2a-e** exhibited any folding characteristics.

Then the attention was drawn towards the possible mode of π- π stackings in the compounds **3a-e** where the amide groups at C-4 position of imidazole rings of each of the AICA derivatives **2a-e** was converted to cyano groups keeping phenyl/*p*-halophenyl substituents as N1 of imidazole moiety intact (Scheme 2). The crystal lattices of **3a-e** revealed the presence of T-stackings along with the *anti* /*syn* π-π stackings of both imidazoles and phenyl/*p*-halophenyl moiety. The unit cells of the lattices of two representative compounds **3a** and **3b**, their T-stacking patterns and *anti*-parallel π-π stackings of imidazole-imidazole and phenyl-phenyl moieties are shown in Fig. 9 and Fig. 10 respectively.

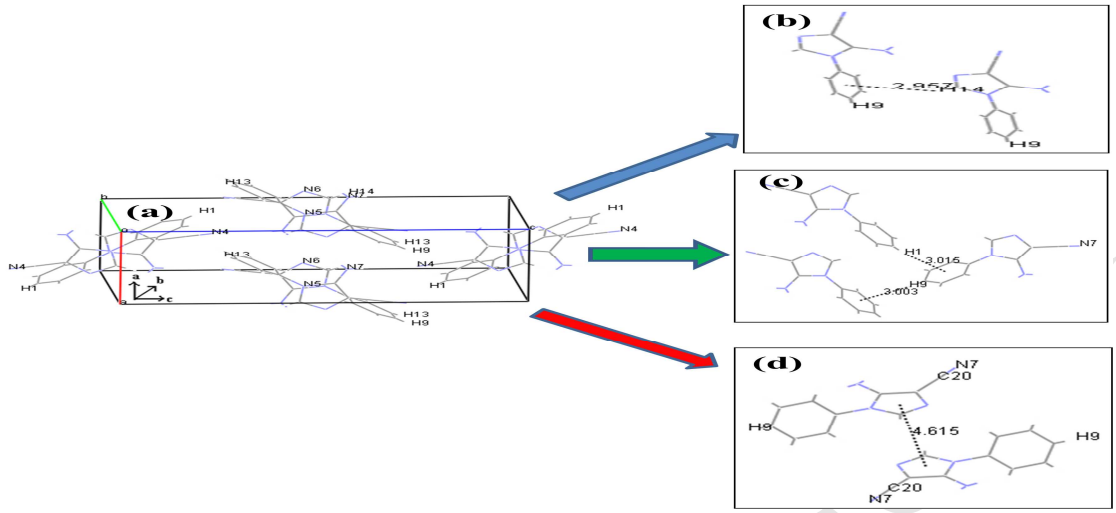

Fig. 9. (a) unit cell arrangement viewing along b-direction, (b) T-stacking between the hydrogen attached with the C-2 position of imidazole and the closest phenyl moiety, (c) T-stacking between the hydrogen attached with the C-4' position of phenyl and the closest phenyl moiety and (d) π- π stacking distance of two *anti*-parallel imidazole-imidazole of compound **3a**

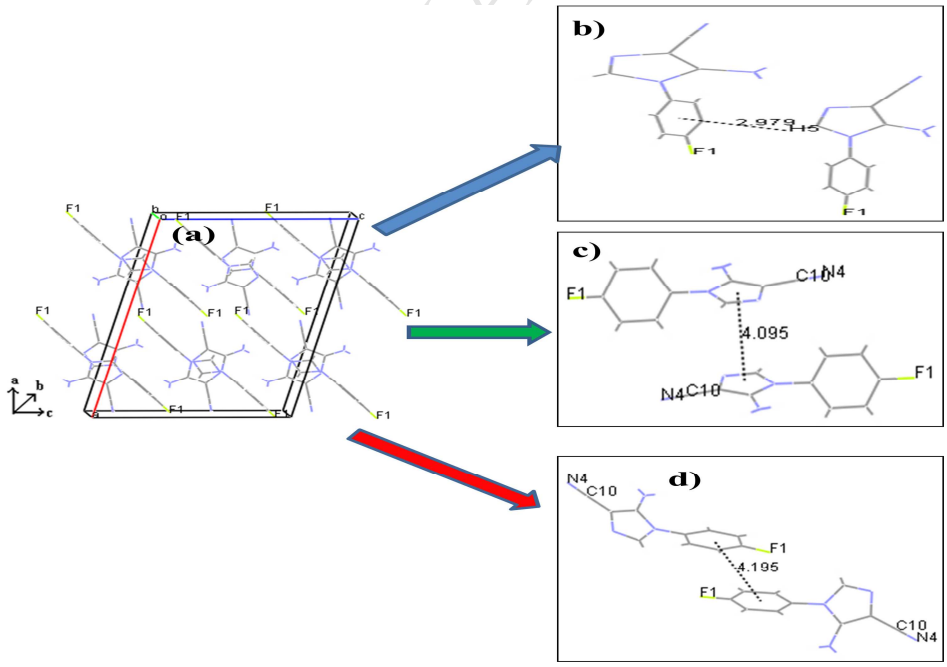

Fig. 10. (a) unit cell arrangement viewing along b-direction, (b) T-stacking distance between the hydrogen attached with the C-2 position of imidazole and the closest *p*-fluorophenyl moiety, (c) π- π stacking distance of two *anti*-parallel imidazoles and (d) π-π stacking distance of two *anti*-parallel *p*-fluorophenyls of compound **3b**.

X-ray crystallographic studies of **3a-e** indicated the presence of imidazole-imidazole PD π-π stacking in *anti*-parallel fashion (Fig. 9d for compound **3a** and Fig. 10c for compound **3b**) in their crystal lattices. *Anti*-parallel phenyl-phenyl PD π-π stackings were observed in the crystal lattices of **3b-e** (Fig. 10d for compound **3b)** whereas similar stacking pattern was not detected in the crystal lattice of **3a.** It was fascinating to note that **3a** showed its differences with **3b-e** in their T-stacking pattern. The crystal lattice of **3a** had shown dual T-stacking interactions. Each of the molecules belonging to the series **3a-e** had specific T-stacking between C2-H of imidazole ring with the closest π-cloud of phenyl moiety (Fig. 9a and Fig. 10a)**.** The crystal lattice of **3a** disclosed additional T-stacking involving C4'-H of N1-phenyl substituent with the closest π-cloud of phenyl moiety (Fig. 9b). This type of extra T-stackings were not identified in the crystal lattices of **3b-e**, since in those molecules the C-4' positions of phenyl substituents at N1 of their imidazole rings were occupied by -F, -Cl, -Br and -I respectively. T-stacking between C2-H of imidazole ring and closest phenyl/*p*-halophenyl ring for the compounds **3a-e** might originate due to the acidic nature of C2-H of imidazole ring caused by the electron-withdrawing effect of –CN group at C4 position**.** T-stacking, *anti*-parallel PD-stacked imidazole-imidazole and phenyl-phenyl π-π stacking interactions of compounds **3c-e** are presented in Supplementary data, Fig.S57-Fig.S59.

Table 5

Anti-parallel PD π-π stacking distances from X-ray crystallographic analysis of **3a-e** and the corresponding vertical π-π stacking distances

Compound	imidazole-imidazole *anti*-parallel π-π stacking			phenyl-phenyl *anti*-parallel π-π stacking		
	π-π stacking distance from X-ray crystallogra-phic lattice(Å)	slip angle from X-ray crystallog-raphic lattice(º)	vertical π-π distance (Å)	π-π stacking distance from X-ray crystallog-raphic lattice(Å)	slip angle from X-ray crystallogr ap-hic lattice(º)	vertical π-π distance (Å)
3a	4.61	4.58	4.59	-	-	-
3b	4.09	5.60	4.07	4.19	35.18	3.42

3c	4.92	7.45	4.88	4.88	43.24	3.55
3d	4.18	36.64	3.35	4.05	7.18	4.12
3e	4.03	32.07	3.41	4.16	7.71	4.12

.

Table 5 tabulates the distances between the centroids of the two closest imidazoles in *anti*-parallel stacking arrangements of **3a-e** and also the distances between PD-stacked *p*-halophenyl–*p*-halophenyl moieties for **3b-e.** Corresponding vertical distances values for each of the PD-stacked imidazole pairs and *p*-halophenyl pairs are reported in Table 5 along with the characteristic slip-angles (shown in Supplementary data, Fig.S43-Fig.S53). The vertical distances which are important for the measurements of the closeness of two PD-stacked moieties are not applicable in T-stacking interactions which involve C-H···π type interactions instead of PD-stacked π-π type. Simultaneously, the closest *syn*-parallel dimers from the crystal lattices of **3a-e** were taken out to obtain the π-π stacking distances between the centroids of the two PD-stacked imidazole units and between the centroids of the two phenyl units. As observed in cases of **2a-e**, both types of PD-stacked arrangements for **3a-e** showed identical distance values in respective cases with explicit differences in slip angles (shown in Table 6). Since the phenyl/*p*-halophenyl unit is attached to N-1 of imidazole with a free-rotable single bond, the lattices showed preference for the torsion angles between imidazole and phenyls to lie in the range of │50.66º│ to │78.36º│ (please see Supplementary data, Table S5) in cases of **3a-e**. Hetero imidazole-phenyl π-π stacking was not possible also in the molecules **3a-e**.

Table 6
Syn-parallel π-π stacking distances from X-ray crystallographic analysis of **3a-e** and the corresponding vertical π-π stacking distances

Compound	imidazole-imidazole *syn*-parallel π-π stacking			phenyl-phenyl *syn*-parallel π-π stacking		
	π-π stacking distance from X-ray crystallogr-aphic lattice(Å)	slip angle from X-ray crystallo-graphic lattice(º)	Vertical π-π distance (Å)	π-π stacking distance from X-ray crystallog-raphic lattice(Å)	slip angle from X-ray crystallogr-aphic lattice(º)	Vertical π-π dista-nce (Å)

3a	6.23	46.50	4.29	6.23	40.93	4.71
3b	6.18	38.22	4.85	6.29	33.97	5.22
3c	6.08	38.88	4.73	6.29	30.42	5.42
3d	6.41	44.03	4.61	6.41	36.33	5.16
3e	6.43	44.16	4.61	6.43	36.92	5.14

Table 7 presents T-stacking distances involving C2-H of imidazaole and the closest π-cloud of phenyl/*p*-halophenyl moieties in the crysyal lattices of **3a-e.** The values were in the range of 2.92-3.16Å and might afford stability to these systems. Another T-stacking was recognized in the crystal lattice of **3a** involving C4'-H of phenyl substituent and the closest π-cloud of phenyl moiety (Fig. 9c) and presented in Table 7**.**

Table 7

T- stacking distances from X-ray crystallographic analysis of **3a-e**

Compound	T-stacking distance between C-2 hydrogen of imidazole and the closest phenyl/p-halophenyl moiety (Å)	T-stacking stacking between C-4'hydrogen of phenyl and the closest phenyl ring (Å)
3a	2.96	3.00, 3.01
3b	2.98	-
3c	2.92	-
3d	3.16	-
3e	3.15	-

T-stacking distances of **3a-e** were the shortest stacking distances than the distances corresponding to *anti*-parallel imidazole-imidazole and phenyl-phenyl stacked moities whereas the *syn* parallel PD-stackings for those molecules recorded the highest values.

3.2. Computational studies on stacking interactions

At an early date, rotational contour analysis of the electronic spectra of *sym*-tetrazine has revealed the presence of two isomers: a planar C-H···N hydrogen bonded dimer and a T-shaped dimer with C-H··· π interactions [52]. Using a combination of two-colour resonant two-photon ionization technique and

Leonard-Jones potential calculation [53], both *syn*-parallel and *anti*-parallel π-stacked and T-stacked varieties of pyrazine-dimers have been reported [52]. As evident from the order of stability of dimers as 1,3,5-triazine> pyrazine> pyridine, reported by Sathamurthy *et. al.*[54], an increase of the number of nitrogen atoms on the heterocyclic ring leads to an increased π-stacking strength. A comparison of energetics of benzene-dimer, benzene-pyridine hetero-dimer and pyridine-dimer with the help of CCSD(T) level of calculation indicates that the introduction of nitrogen to replace the carbon atom of benzene creates a dipole along with reduction of spatial extent of π cloud and polariziability of hetero-aromatic moiety comparative to benzene [52,54,26]; the stabilization in the case of pyridine dimer has shown to be of the order of 1.43 Kcal mol^{-1} higher than the benzene dimer [26,54] . It is also to note that the results of *ab-initio* calculations on the benzene-dimers depend on the selection of basis set to some extent [42,55]. A detailed understanding of the extent of stabilization offered by different π-π stacking and T-stacking interactions of compounds **2a-e** and **3a-e** was correlated with the results of DFT calculations. For compounds **2a-e**, DFT studies were focused on PD-stacked (a) *anti*/*syn*-parallel imidazole pairs and (b) *anti*/*syn*-parallel phenyl pairs occurring simultaneously in their crystal lattices. For the consideration of *anti*-parallel stackings the studies had focused on the closest pairs of such *anti*-parallel imidazoles in void and also such closest pair of *anti*-parallel phenyls/*p*-halophenyl in void , in the respective cases, by way of proper selection out of X-ray crystallographic packing keeping the mode of π-π stacking as well as the slip angle intact (Table 2 and Table 3). This would afford the optimized form of the respective dimer at once. In a cue, detailed DFT calculations of the optimized energies of dimers using the basis set mpwb95/6-31++g for **2a-d** and mpwb95/lanl2dz [56] for **2e** had been pursued by keeping the slip-angle of π-π stacked dimers unaltered while adopting gradual change of π-π stacking distance parameter. Subsequently, the π-π -stacking energy corresponding to each set of calculations for a given π-π distance is computed from the Equation 2**.**

π-π stacking energy= (optimized energy of the dimer) - 2x (optimized energy of the monomer)**…..**Equation 2

The optimized energy of the monomer, remaining the same for the *anti*-parallel conformations of imidazoles as well as phenyl/*p*-halophenyl, had been separately calculated by using the same basis sets mpwb95/6-31++g for **2a-d** and mpwb95/lanl2dz for **2e**. The crystallographic CIF was used to generate the initial geometery of the stacked dimer and monomer. Afterthat, single point energy had been calculated using DFT method. Here 'optimized geometry' indicates actually the geometry which had already been optimized by X-ray crystallographic analysis in the solid state. This calculated π-π stacking energy corresponded to simple π-π stacking situation only, infact unmixed with other possible interactions like hydrogen bonding. Here mpwb95/6-31++g and mpwb95/lanl2dz basis sets were used since these correspond to correlation consistent methods [56,57] and included the features of diffusion correction as was appropriate for these types of π-π stacking calculations considered up to a long stacking distance (total data of the calculations have been tabulated in Supplementary data, Table S6-S13). A graph was drawn by plotting the π-π -stabilization energy data against variable π-π -stacking distance. DFT calculations on π-π stacking of representative compounds **2c** and **2e** are shown in Fig. 11 and Fig. 12 (DFT calculations on π-π stacking of compounds **2a**, **2b** and **2d** are shown in Supplementary data, Fig. S60-Fig.S62). Fig. 11b represents π-π -stacking distance of two imidazoles in *anti*-parallel orientation of representative compound **2c** as appeared in its crystal lattice. Fig. 11c shows DFT-generated curve of π-π -stacking energies *vs.* variable π-π stacking distances as computed for the compound **2c**. Similarly for corresponding *anti*-parallel phenyl/*p*-halophenyl stacking, Fig. 11d and Fig. 12b exhibit π-π -stacking distances obtained from the crystal lattices of **2c** and **2e** respectively and Fig. 11e and Fig. 12c indicate DFT-generated curve of compound **2c** and **2e** respectively.

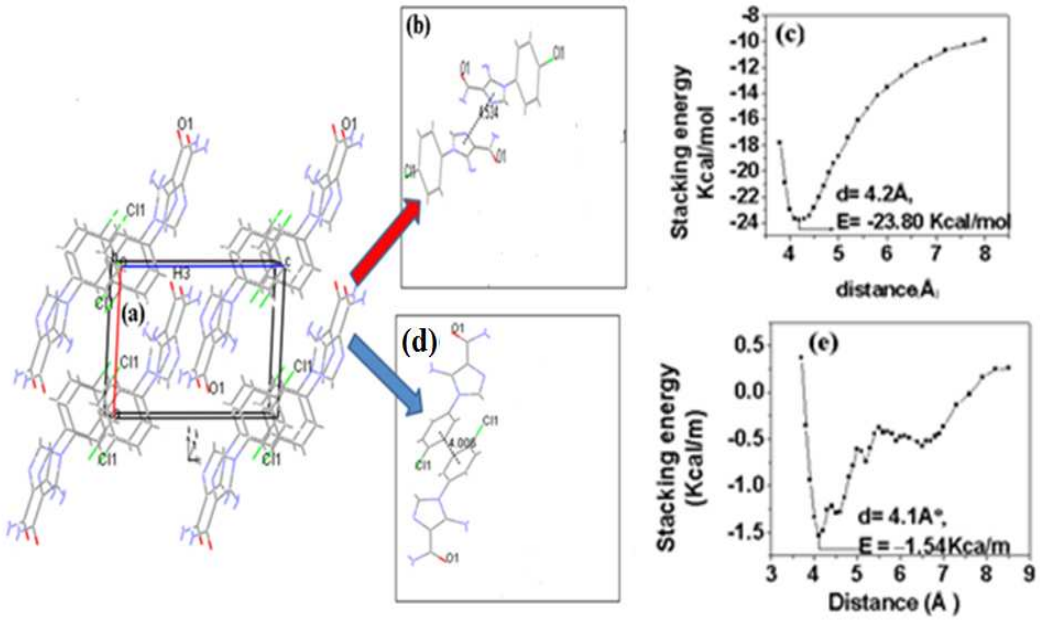

Fig. 11. (a) unit cell arrangement viewing along b-direction, (b) π- π stacking distance of two *anti*-parallel imidazoles, (c) the plot of π- π stacking distance of *anti*-parallel imidazoles, (d) π- π stacking distance of two *anti*-parallel *p*-chlorophenyls and (e) the plot of π- π stacking distance of two *anti*-parallel *p*-chlorophenyls, corresponding to compound **2c**

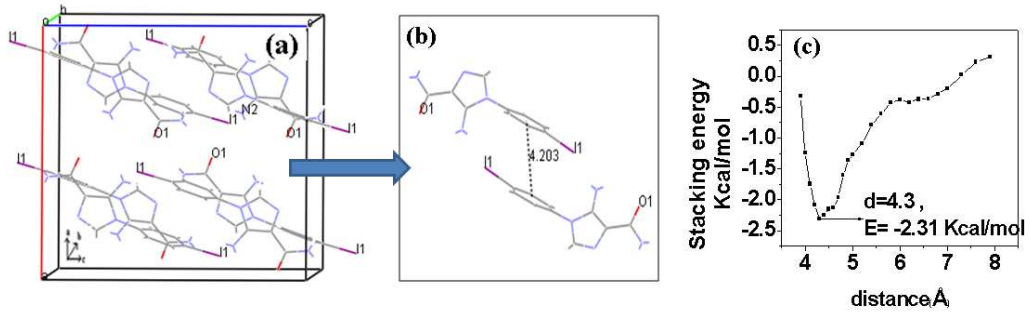

Fig. 12. (a) unit cell arrangement viewing along b-direction, (b) π- π stacking distance of two *anti*-parallel *p*-iodophenyls and (c) the plot of π- π stacking distance of two *anti*-parallel *p*-iodophenyls, corresponding to compound **2e**

Thus maximum stacking stabilization energies corresponding to the minimum π-π -stacking distances are known from the curve generated by DFT calculations. Table 8 furnishes an effective comparison of *anti*-parallel π-π stacking distances of imidazoles pairs of **2a-c** with those deduced from DFT calculations.

Table 9 tabulates similar comparisons for *anti*-parallel π-π stacking distance of phenyls/*p*-halophenyls of **2a-e.**

Table 8
Comparison of PD π-π stacking distances for the *anti*-parallel pairs of imidazoles of **2a-c** obtained from X-ray crystallographic and DFT studies

Compound	π-π stacking distance(Å) from X-ray crystallographic analysis	min. π-π stacking distance(Å) obtained from DFT calculations	stacking energy (Kcal-mol^{-1}) from DFT calculations
2a	4.53	4.3	-12.80
2b	4.43	4.2	-11.94
2c	4.53	4.2	-23.80

Table 9
Comparison of PD π-π stacking distances for the *anti*-parallel pairs of phenyls of **2a-e** obtained from X-ray crystallographic and DFT studies

compound	π-π stacking distance(Å) from X-ray crystallographic analysis	min. π-π stacking distance(Å) obtained from DFT calculations	stacking energy (Kcal-mol^{-1}) from DFT calculations
2a	4.14	4.2	-2.90
2b	4.46	4.4	-3.84
2c	4.01	4.1	-1.54
2d	4.04	3.8	-12.81
2e	4.2	4.3	-2.31

Comparisons of the data, presented in Table 8 and Table 9**,** reveal that stacking energies for *anti*-parallel π- π stackings of imidazole pairs are in the range of 11.94 to 23.80 Kcal mol^{-1} whereas the *anti*-parallel π-π stacking energies of phenyl/*p*-halophenyl pair are much less viz.1.54-3.84 Kcal mol^{-1} with the exception

of *p*-bromophenyl-AICA **(2d)** having an oddly high value of 12.81 Kcal mol^{-1}. Studies on *syn*-parallel stackings of respective imidazole pairs and phenyls/*p*-halophenyl pairs were also undertaken. Compound **2b** possessing fluorine at the 4'-position of aromatic ring was chosen. The closest pair of imidazoles and that of *p*-fluorophenyls are taken out from the crystal lattice (shown in Fig. 13a) as the optimized pairs (Fig. 13b). As discussed earlier, π- π stacking distances for both *syn*-parallel imidazole pair and *syn*-parallel *p*-fluorophenyl are the same and the value is 7.66Å. DFT calculations were performed keeping slip-angle description unaltered while adopting gradual change of π- π stacking distance parameter. Afterwards, the apparent π-π stacking energies were computed from the Equation 2 and plotted against π-π stacking distances to get the curve (Fig. 13c).

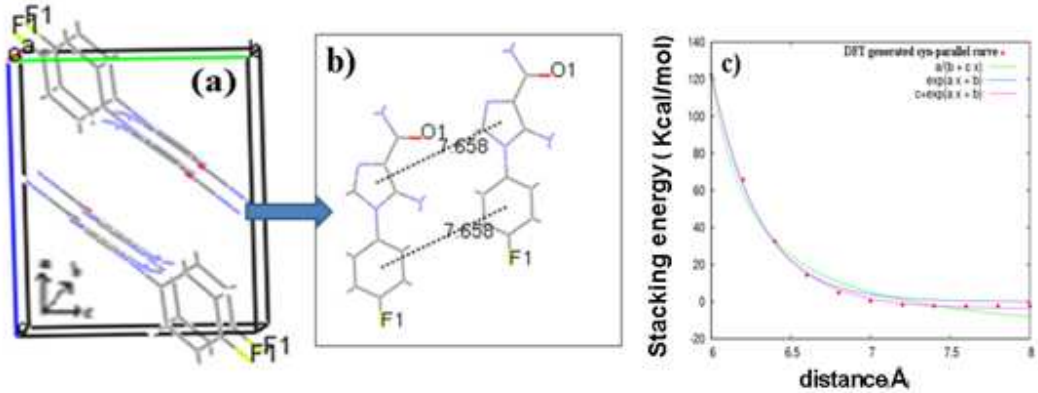

Fig. 13. (a) unit cell arrangement viewing along a-direction, (b) π- π stacking distances of two *syn*-parallel imidazoles and *syn*-parallel *p*-fluorophenyls in the lattice and (c) the plot of π- π stacking energies against varying π- π stacking distance of *syn*-parallel dimer, corresponding to compound **2b** (slip angle kept intact as observed in X-ray crystallographic lattice).

It should be mentioned here that for *syn*-parallel stackings, not only the respective imidazole pairs and *p*-fluorophenyl pairs reinforce their stacking mutually, hydrogen bonding and other weak forces also contribute to the stability of *syn*-parallel dimer system. The graph would be of an exponential nature and can be attempted for fitting with the use of gnuplot; taking the help of the following three possible functions (errors quoted are '1σ' errors).

(i) F1(x) = a + [c/(x+b)] with best fit values where a = -24.4634 +/- 4.647 (19%), b = -5.75052 +/- 0.03847 (0.669%), c = 37.0125 +/- 6.424 (17.36%) and reduced chi-square = 26.1556,

(ii) F2(x) = exp (a x + b) with best fit values where a = -3.44684 +/- 0.1632 (4.736%), b = 25.5005 +/- 0.9679 (3.796%) and reduced chi-square = 9.42956,

(iii) F3(x) = c + exp (a x + b) with best fit values where a = -3.14733 +/- 0.07875(2.502%), b = 23.7276 +/- 0.4639 (1.955%), c = -3.80906 +/- 0.6201 (16.28%) and reduced chi-square = 1.74827

The asymptotic part of the curve starts from a PD π-π distance of 7.6 Å and this appeared to be almost same with the π-π stacking distance of 7.66 Å observed in the crystal lattice of **2b**. The graphically calculated π-π stacking energy was -2.42Kcal mol^{-1} which included all types of non-covalent interactions. To ascertain the similar correlation between X-ray crystallographic data and DFT calculated results in case of **3a-e**, the studies were focused on (a) T-stacking between C2-H of imidazole and the closest phenyl/*p*-halophenyl moiety for **3a-e** with an additional T-stacking between C4´-H of imidazole and the closest phenyl moiety in **3a** as well as (b) π-π stacking between parallel-displaced *anti* -parallel imidazole and (c) *anti* -parallel phenyl pairs involving gradual changes of C-H···π and π-π stacking distance parameters respectively. The optimized energy of the monomer of **3a-e** was calculated by using the basis set mpwb95/6-31++g for **3a-d** and mpwb95/lanl2dz for **3e.** DFT calculations on T-stacking and π-π stacking of representative compounds **3a** and **3c** are shown in Fig. 14 and Fig. 15 (DFT calculations on T-stacking and π-π stacking of compounds **3b, 3d** and **3e** are shown in Supplementary materials, Fig. S63-Fig.S65). Fig. 14b and Fig. 15b show the T-stacking distances between C2-H of imidazole and the closest phenyl/*p*-halophenyl moiety of representative compounds **3a** and **3c** respectively while Fig. 14d indicates the T-stacking distance between C4´-H of phenyl and the closest phenyl moiety of **3a** as revealed from their respective crystal lattices and corresponding Fig. 14c, Fig. 14e and Fig. 15c specify the curves of T-stacking energy *vs.* variable T -stacking distance obtained from the DFT calculation. Fig. 14f and

Fig. 15d show π-π -stacking distances of PD-stacked *anti*-parallel imidazole pairs and corresponding Fig. 14g and Fig. 15e indicate the relevant curves for DFT calculated π-π -stacking energies *vs.* variable π-π -stacking distances for compounds **3a** and **3c** respectively. Fig. 15f gives π-π -stacking distance for *anti*-parallel *p*-chlorophenyl pairs in the crystal lattice of **3c** and Fig. 15g shows the respective DFT-generated curve for the variables as stated in all previous cases.

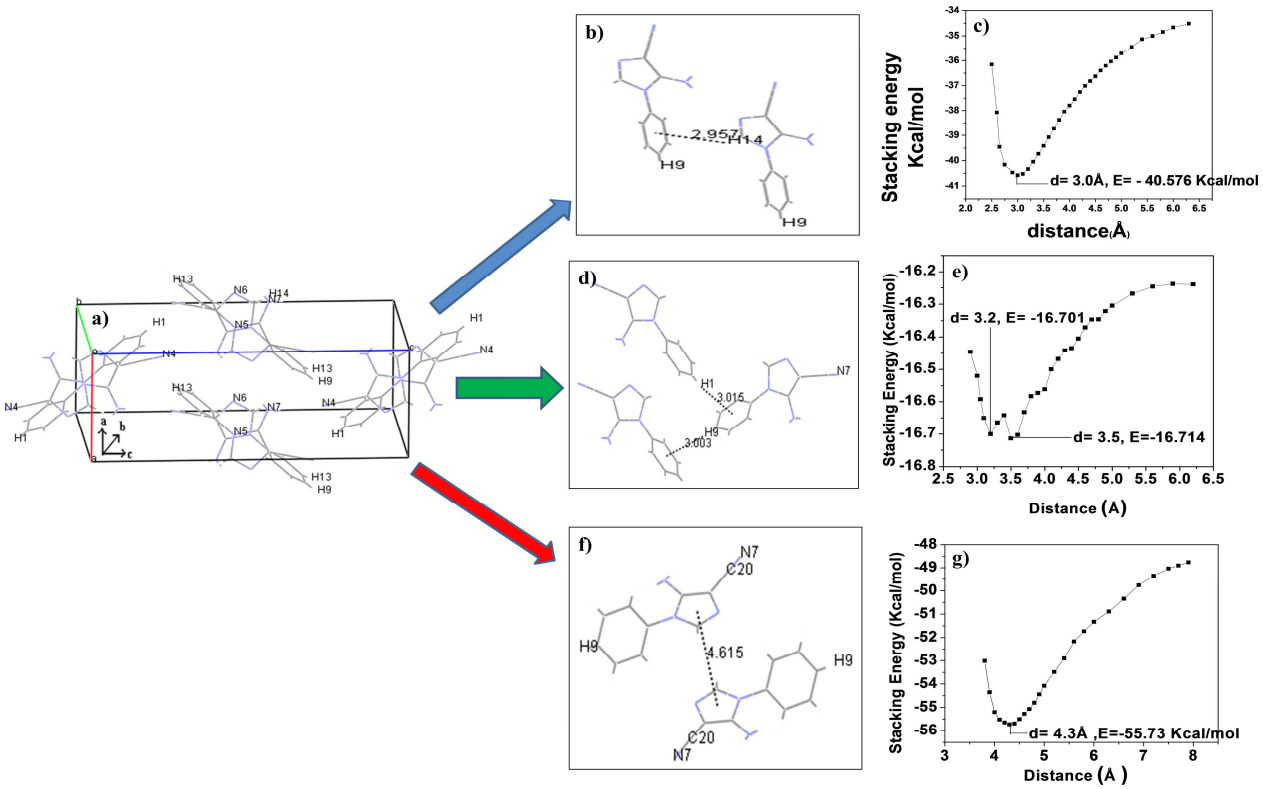

Fig. 14. (a) unit cell arrangement viewing along b-direction, (b) T-stacking distance between the hydrogen attached with the C-2 position of imidazole and the closest phenyl moiety, (c) the plot of the T-stacking energies against varying T-stacking distances between the hydrogen attached with the C-2 position of imidazole and the closest phenyl moiety, (d) T-stacking distance between the hydrogen attached with the C-4' position of phenyl and the closest phenyl moiety, (e) the plot of T-stacking energies against varying T-stacking distances between the hydrogen attached with the C-4' position of phenyl and the closest phenyl moiety, (f) π- π stacking distance of two *anti*-parallel imidazoles and (g) the plot of the π- π stacking energies against varying π- π stacking distance of two *anti*-parallel imidazoles, corresponding to compound **3a**

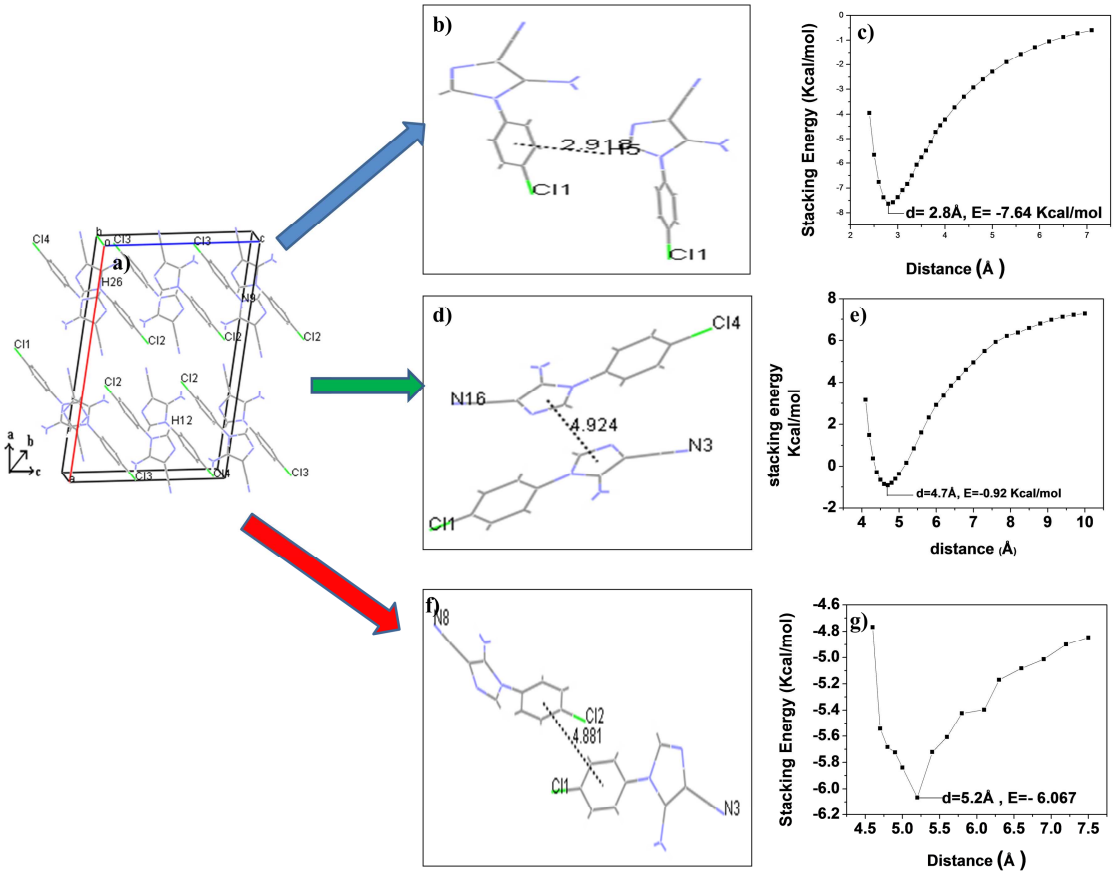

Fig. 15. (a) unit cell arrangement viewing along b-direction, (b) T-stacking distance between the hydrogen attached with the C-2 position of imidazole and the closest *p*-chlorophenyl moiety, (c) the plot of the T-stacking energies against varying T-stacking distances between the hydrogen attached with the C-2 position of imidazole and the closest *p*-chlorophenyl moiety, (d) π- π stacking distance of two *anti*-parallel imidazoles, (e) the plot of the π- π stacking energies against varying π- π stacking distances of two *anti*-parallel imidazoles, (f) π-π stacking distance of two *anti*-parallel *p*-chlorophenyls and (g) the plot of the π- π stacking energies against varying π- π stacking distances of two *anti*-parallel *p*-chlorohenyls, corresponding to compound **3c**

Total data of the DFT calculations of compounds **3a-e** have been tabulated in Supplementary data, Table S15-S29). Table 10 displays all the data relating to both types of T-stackings observed in the molecules **3a-e** including the specific one manifested in case of **3a** which was absent in **3b-e**.

Table 10
Comparison of T-stacking distances between C2-H of imidazole and the closest phenyl/*p*-halophenyl moieties obtained from X-ray crystallographic and DFT studies of **2a-e**

Compound	T-stacking between C2-H of imidazole and the closest phenyl/*p*-halophenyl moities			T-stacking between C4´-H of imidazole and the closest phenyl/*p*-halophenyl moities		
	T-stacking distance(Å) from X-ray crystallograp-hic analysis	T-stacking distance (Å) obtained from DFT calculation	Stacking energy (Kcal-mol^{-1}) from DFT calculation	T-stacking distance (Å) from X-ray crystall-ographic analysis	T-stacking distance (Å) obtained from DFT calculation	stacking energy (Kcal-mol^{-1}) from DFT calculation
2a	2.96	3.0	-40.58	3.00, 3.01	3.2, 3.5	-16.70, -16.71
2b	2.98	2.9	- 7.56	-	-	-
2c	2.92	2.8	-7.64	-	-	-
2d	3.16	3.1	-10.53	-	-	-
2e	3.15	3.1	-8.04	-	-	-

A comparison between the observed π-π stacking distances for *anti*-parallel pairs of imidazoles and related DFT computational data for the compounds **3a-e** is presented in Table 11. Table 12 tabulates analogous comparison for *anti*-parallel π-π stacking involving phenyls/*p*-halophenyls pairs of compounds **3b-e**.

Table 11

Comparison of PD π-π stacking distances of the *anti*-parallel pairs of imidazoles obtained from X-ray crystallographic and DFT studies of **3a-e**

Compound	π-π stacking distance(Å) from X-ray crystallographic analysis	π-π stacking distance(Å) obtained from DFT calculation	stackingenergy (Kcal-mol^{-1}) from DFT calculation
3a	4.61	4.3	-55.73
3b	4.09	3.75	-11.50
3c	4.92	4.7	-0.92
3d	4.18	4.1	-9.54
3e	4.03	3.9	-9.60

Table 12

Comparison of PD π-π stacking distances for the *anti*-parallel pairs of phenyls/*p*-halophenyls obtained from X-ray crystallographic and DFT studies of **3b-e**

Compound	π-π stacking distance(Å) from X-ray crystallographic analysis	π-π stacking distance(Å) obtained from DFTcalculation	stackingenergy (Kcal-mol^{-1}) from DFT calculation
3b	4.19	4.3,4.7	-1.25, -1.26
3c	4.88	5.2	-6.07
3d	4.05	3.8	-9.94
3e	4.16	4.15	-1.62

*3.3. Skew-syn and skew-anti arrangements of **2b** and **2c** vis-à-vis computational study*

Compounds **3a**, **3d** and **3e** had shown normal *anti* and *syn* parallel arrangements in their crystal lattices where dihedral angels were 0º and 180º for *syn* and *anti* arrangements (please see Supplementary data, Fig.S66 and Fig.S67). However, the compounds **3b** and **3c** with flourine and chlorine respectively at 4'-

position of the aromatic substituent on N1-imidazole ring had shown different behaviours with respect to other derivatives. In their crystal lattices, the π-π stacked phenyl rings did not make 0º and 180º dihedral angles in their *syn*-parallel and anti-parallel arrangements. Hence instead of describing them as *syn* and *anti* nomenclatures, arrangements in crystal lattices of **3b** and **3c** were categorized as skew-*anti* and skew-*syn*. Fig. 16 and Fig. 17 show skew-*syn* and skew-*anti* orientation in the crystal lattices of **3b** and **3c** respectively.

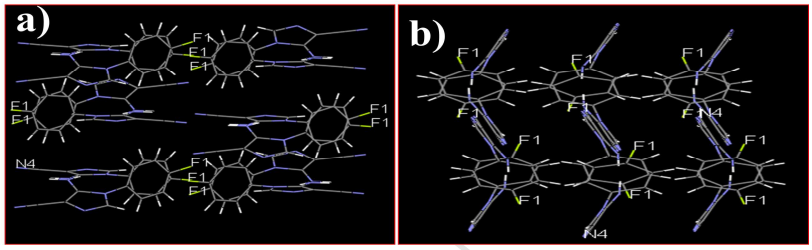

Fig. 16. a) and b) show skew-*syn* and skew-*anti* orientation respectively in the crystal lattice of **3b**

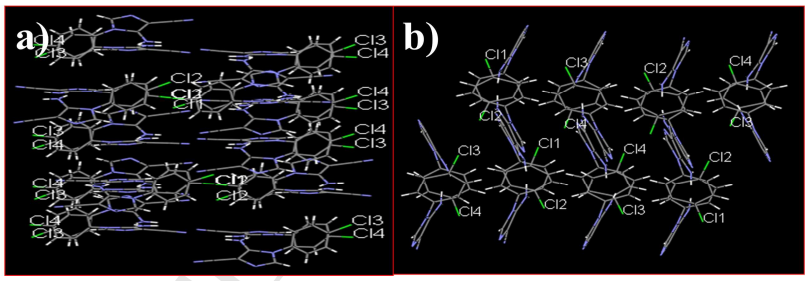

Fig. 17. a) and b) show skew-*syn* and skew-*anti* orientation respectively in the crystal lattice of **3c**

X-ray crystallographic studies had shown that the dihedral angels of skew-*syn* and skew-*anti* orientation of **3b** were 29.25º and 149.54º (Fig. 18) respectively and the dihedral angles of skew-*syn* and skew-*anti* orientation of **3c** were 41.27º and 136.35º respectively (Fig.19).

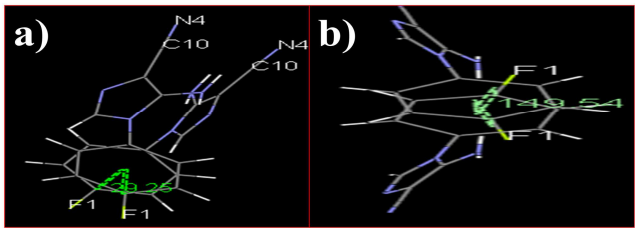

Fig. 18. a) and b) show dihedral angles of skew-*syn* and skew-*anti* orientation of **3b**

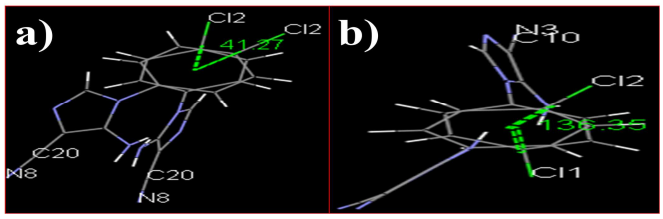

Fig. 19. a) and b) show dihedral angles of skew-*syn* and skew-*anti* orientation of **3c**

To establish correlation between the dihedral angle values obtained from X-ray crystallographic data with the results of DFT calculations, the strategy was to calculate the energy of the dimer by adopting gradual change of dihedral angle parameter and to compare those computed energies with X-ray crystallographic results using **Gaussian 09W** where mpwb95/6-31++G was used as basis set. Dihedral angle value at the minimum of the graph obtained from DFT calculated results indicated most stable π-π stacking association, corresponding to the optimized dihedral angle in each case of crystal lattice for skew-*syn* and skew-*anti* dispositions exhibited in the molecules **3b** and **3c**. Graphical representation of the correlation between the DFT calculated optimized dihedral angel and X-ray crystallographic results for skew-*syn* arrangement in **3b** and skew-*syn* and skew-*anti* dispositions in **3c** are shown in Fig. 20 and Fig. 21 respectively (total data of DFT calculation are shown in Supplementary data, Table S30-S32).

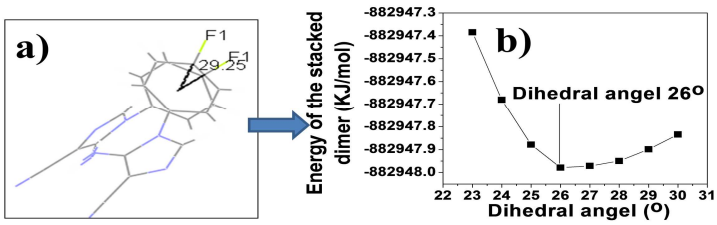

Fig. 20. a) shows dihedral angel for skew-*syn* orientation of **3b** obtained from X-ray crystallographic analysis and b) shows plot of energy of the stacked dimer against varying dihedral angel parameter (keeping slip angel intact).

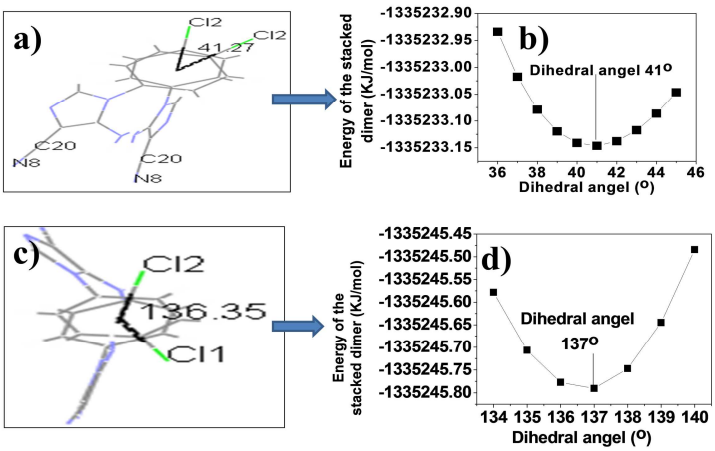

Fig. 21. a), b) show dihedral angel for skew-*syn* orientation and skew-*anti* orientation of **3c** obtained from X-ray crystallographic analysis and b), d) show plot of energy of the stacked dimer against varying dihedral angel parameter (keeping slip angel intact).

In each case, DFT calculated values were in good agreements with the X-ray crystallographic results (shown in Table 13).

Table 13
Comparison table of dihedral angel obtained from X-ray crystallographic results and DFT-calculatios for **3b** and **3c**

Compound		**3b**	**3c**
Dihedral angel for skew-*syn* orientattion	Dihedral angel obtained from X-ray crystallographic result (°)	29.25	41.27
	DFT-calculated optimized dihedral angel (°)	26	41
Dihedral angel for skew-*anti* orientattion	Dihedral angel obtained from X-ray crystallographic result (°)	149.54	136.35
	DFT-calculated optimized dihedral angel (°)	-	137

*3.4. Halogen-halogen interaction and molecular channel formation of **2a-e** and **3a-e***

Compounds **2d** and **2e** had shown halogen-halogen soft interactions in their crystal lattices. Although there exist two types of halogen-halogen soft interactions, both **2d** and **2e** display type-I interaction only. This type-I interaction is characterized by an inter-halogen distance being generally less than the sum of van der Waals radii of two halogens involved and a symmetrical array of R-X_1···X_2-R with $\theta_1=\theta_2$ (where θ_1 and θ_2 are the R-X_1···X_2 and X_1···X_2-R angles respectively). Although there exists disagreement about the exact nature of the halogen-halogen interaction, it has to be governed by attractive forces [11,58] or by minimization of repulsive forces [59-62]. DFT studies [63] have indicated that the most stabilizing situations correspond to $\theta_1=\theta_2 \approx 150$ and the efficiency of the halogen-halogen soft interaction decreases in the order I···I>Br···Br>Cl···Cl. In the crystal lattices of **2e** the I···I distance and the $\theta_1=\theta_2$ angles had been found out to be 3.705 Å and 159.5˚ respectively (Fig. 22a) whereas the corresponding values in case of **2d** are 3.937 Å and 138.68˚(Fig. 22b). These values indicated clearly that the I···I interactions was more effective in case of **2e** than that of the Br···Br interaction in case of **2d**. Such halogen-halogen interaction had not been observed in the lattices of **2c** or **2b** where the corresponding halogen, chlorine or fluorine, was more electronegative. This effective halogen-halogen interaction had possibly led to the formation of molecular channels lined with bromines in the lattice of **2d** (Fig. 22d) and those lined with iodines and carboxamido moieties (Fig. 22c) in the lattice of **2e**.

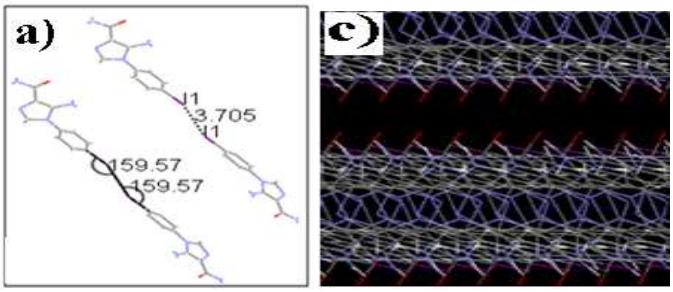

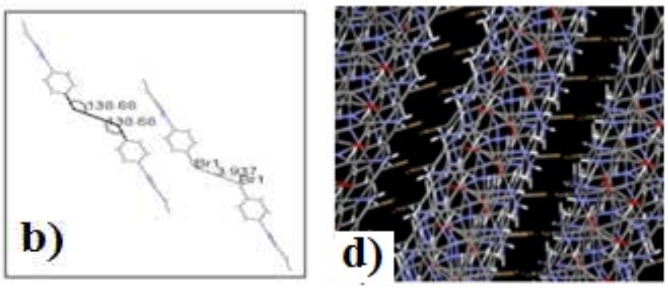

Fig. 22. a) and d) show halogen-halogen distances and C-X···X angles for **2e** and **2d** respectively ; c) and d) show molecular channels in the lattices of **2e** and **2d** respectively.

Type-II halogen-halogen soft interaction had been observed in the crystal lattice of **3d**. In the crystal lattice of **3d,** the Br···Br distance and the θ_1 and θ_2 angles were measured as as 3.95 Å, 158.87˚and 87.44º respectively (Fig. 23a, Fig. 23b). Such halogen-halogen interactions were not identified in the lattices of **3b**, **3c** and **3e** where the corresponding halogens were fluorine, chlorine and iodine respectively. This effective halogen-halogen interaction has led to the formation of molecular channels in the lattice of **3d** along c-direction (Fig. 23c).

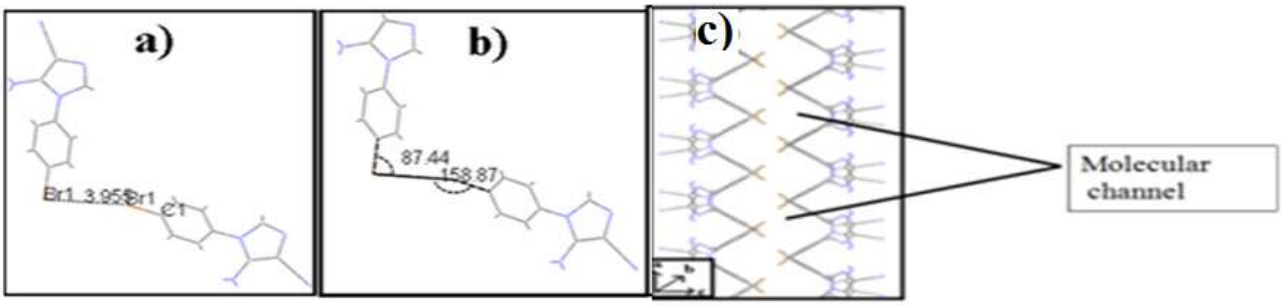

Fig. 23. a) and b) show halogen-halogen distances and C-X···X angles for **3d** respectively, c) shows dihedral angles of C_1-Br_1···Br_1-C_1 for **3d**, d) shows molecular channels in the lattices of **3d** along c-direction.

Although halogen-halogen soft interaction was absent in case of **3e**, it had shown molecular ordering in its lattice generating arrays of the molecular channels along c-direction (shown in Fig. 24)

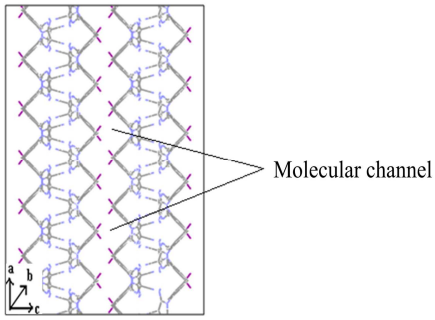

Fig. 24. Molecular channel arrangement in the lattices of **3e** along c-direction.

3.5. Nanostructural behaviour

During the years of new millennium, one dimensional (1-D) organic nano-materials based on small molecules, have attracted great attention, specially for the electronic and optoelectronic devices [64]. 1-D organic nano-structures have been very efficiently constructed with the help of their π-π stacking [65] and/or hydrogen bonding [67] properties. Nano-structural materials like tubes [67], rods [68] or belts [69] have been under extensive investigations due to their properties, much different from their bulk versions. Reportedly a 1-D assembly can be obtained very easily by dispersing a concentrated solution of a 'promising' nano-material into a 'poor solvent'[70].

Single crystal X-ray crystallographic studies of series of 5-amino-1-(phenyl/*p*-halophenyl)imidazole-4-carboxamides **(2a-e)** and 5-amino-1-(phenyl/*p*-halophenyl)imidazole-4-carbonitriles (**3a-e**) had shown different modes of π-π stacking interactions, extensive hydrogen bonding network and soft halogen-halogen interactions. These observations indicated to investigate the formation of nano-structural behaviour of those compounds. To explore the influence of solvent polarity on morphology, the morphological heterogeneity experiments of the compounds **2a-e** and **3a-e** using different solvent systems with the change of polarities had been performed. Scanning electron microscopic (SEM) studies revealed that **2a-e** and **3a-e** had given self-assembled nanostructures in non-polar solvent benzene only. The self-assembled morphological heterogeneity had been checked by preparation of the sample through dispersing the compounds (5Mm) by way of sonication for 2 hours at room temperature in a series of solvents such

as pet ether, methanol, acetonitrile and benzene. The respective solution was allowed to drop on glass cover slips and allowed to dry slowly for 48 hours. Then the SEM images were taken. SEM images revealed that the formation of 1-D nanostructures had been successfully constructed for **2a-c**, and **3a-e** in benzene except **2d** which formed nano-vesicles in this particular solvent benzene. Minimum widths of nano-rod in benzene had been found to be ~92.0nm, 111.57nm, 90nm and 268.70nm for **2a-c** and **2e** respectively (Fig. 25). The SEM images of nano-rod formation are shown in Fig. 25.

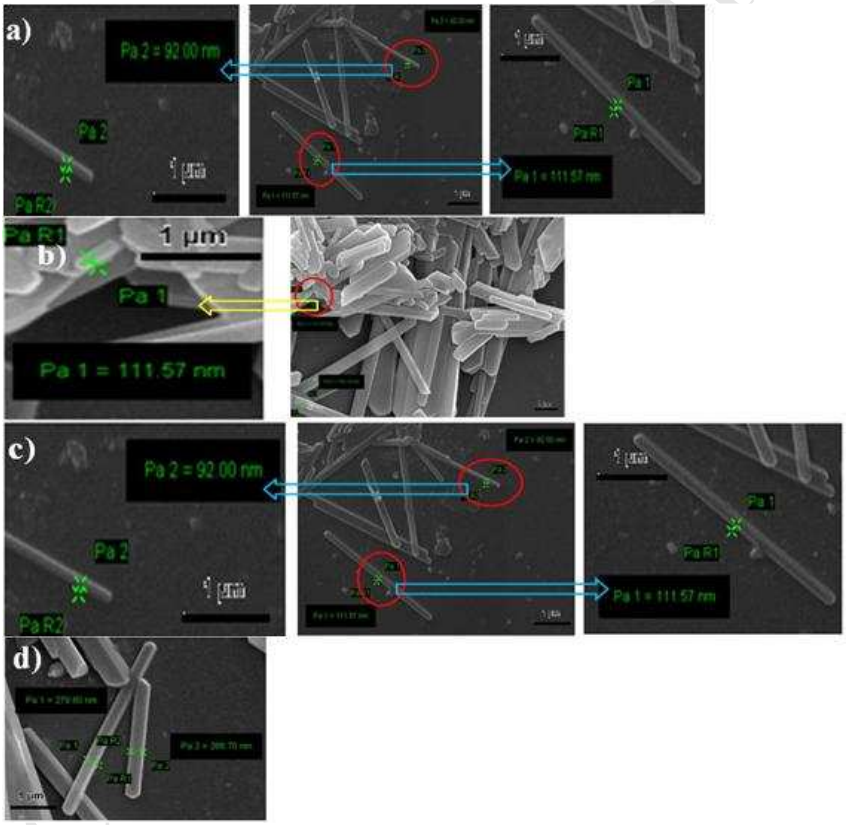

Fig. 25. a), b), c) and d) show SEM images as nano-rods arising from **2a**, **2b**, **2c** and **2e** in benzene

Although, nano-rod morphologies had been observed for **2a-c** and **2e** in benzene, **2d** formed nano-vesicle morphology in benzene having size distribution ~39nm (Fig. 26).

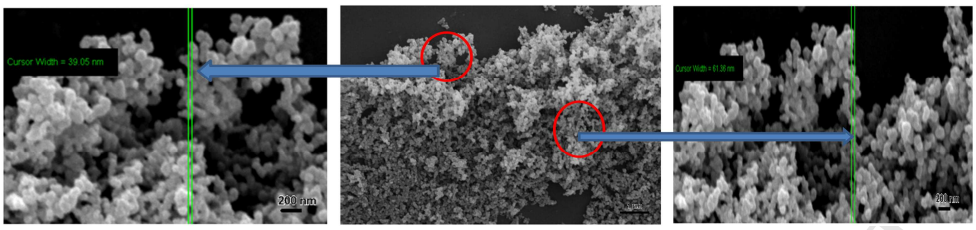

Fig. 26. SEM images of **2d** in benzene

1-D nanostructure morphology was also viewed for **3a-e** in benzene. Minimum widths of nano-rod in benzene were found to be ~155.86nm, 276.24nm, 70.56nm, 94.67nm and 138.01nm for **3a**, **3b**, **3c, 3d** and **3e** respectively (shown in Fig. 27).

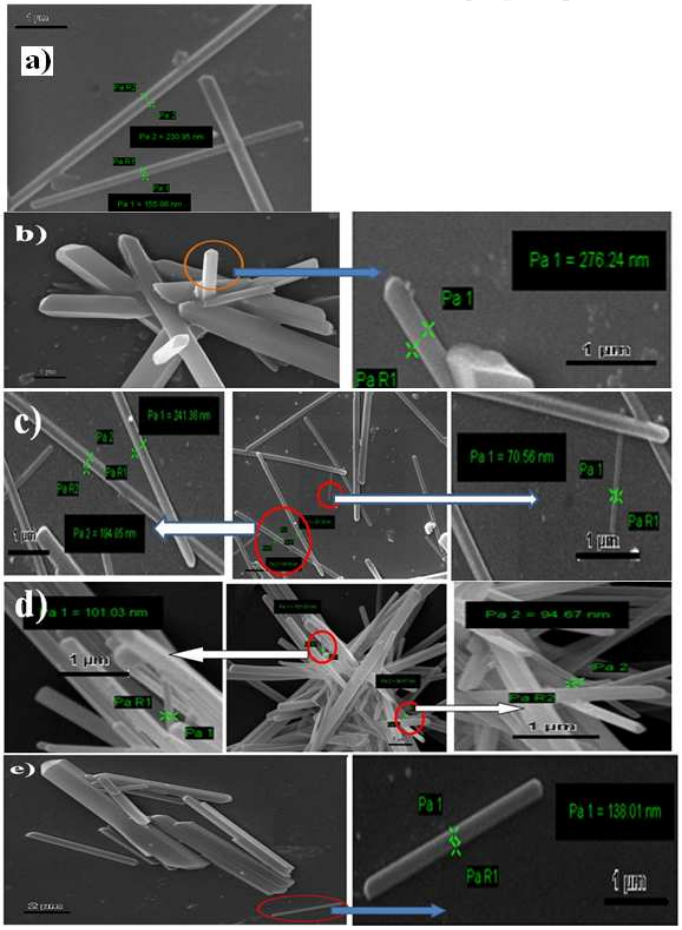

Fig. 27. a), b), c), d) and e) show SEM images as nano-rods arising from **3a, 3b, 3c**, **3d** and **3e** in benzene

4. Conclusion

In conclusion I had successfully chosen a composite system of imidazole, characteristic of an AICA, with a phenyl/*p*-halophenyl substituent at N-1 so that the imidazole and the phenyl together constitute a free-rotable system. All the four halogens (F,Cl,Br,I) had been considered as the *p*-substituents of phenyl to unravel the profound effect of halogens on the supramolecular architecture in the lattices of the compounds by way of their X-ray crystallographic and DFT studies. In their crystal lattices, phenyl/*p*-fluorophenyl/*p*-chlorophenyl compounds **2a-c** had shown *anti*-parallel imidazole-imidazole stack-formations. On the other hand, *p*-bromo/*p*-iodophenyl compounds **2d**, **2e** avoided such *anti*-parallel imidazole-imidazole stacking in their crystal lattices. Each of **2a-c** and **2e** had shown *anti*-parallel phenyl-phenyl π-π stacking of PD-type; **2d** (with bromo as the halogen) indicated *anti*-parallel Sandwich stacking, a choice appearing unusual from the standpoint of stabilization. Compounds **3b-e** had shown T-stacking interactions along with *anti*-parallel PD-type imidazole-imidazole and phenyl-phenyl π-π stacking as well as specifically compound **3a** revealed dual T-stackings interactions along with *anti*-parallel PD-type interaction involving imidazole-imidazole stacking. Halogen-halogen soft interactions and formation of molecular channels were found to play an important role in the series of our compounds. In each of the cases of π-π *anti*-parallel and T-stacking arrangements, DFT studies had been taken up for the purpose of quantification of the π-π stacking and T-stacking stabilization energy. Detailed DFT calculations of the optimized energies of the dimer had been undertaken by taking out the closest stacked pair from the lattice and gradually changing the stacking distance parameter. When the graph of stacking energy *vs.* stacking distance was analyzed, minimum of the curve corresponded to the stacking energy of the dimer. In each case, DFT calculated results were in good agreements with X-ray crystallographic results. Similar DFT studies on simultaneous *syn*-parallel imidazole and phenyl dimer systems corresponded to no π-π stacking stabilization at all. Nano-structural behaviour of compounds **2a-e** and **3a-e** had been observed in non-polar

solvent benzene. Compounds **2a-c**, **2e** and **3a-e** had shown excellent -D nano-structural properties but **2d** had shown nano-vesicle morphology in benzene.

Acknowledgements

The author thanks the University of Calcutta for providing laboratory and spectroscopic facilities. I thank Prof. (retd.) Sibdas Ray, Dr. Kaliprasanna Dhara, Dr. Mehboob Alam, Dr. Aniruddha Ganguly of Chemistry Dept., C.U. and Dr. Shamayita Ray of Physics Dept., C.U. for their support. The author (A. D.) thanks the Council of Scientific and Industrial Research (CSIR), New Delhi, India for the award of a Senior Research Fellowship. Single X-ray Crystallographic studies have been performed with Single Crystal Diffractometer Facilities offered by DST-FIST programme, at the Chemistry Dept., C.U.

Appendix A. Supplementary materials

Supplementary data associated with this article can be found, in the online version, at (http:……..).

References

[1] S. Iijima, Helical microtubules of graphitic carbon, Nature 354 (1991) 56-58.

[2] Z. W. Pan, Z. R. Dai, Z. L. Wang, Nanobelts of Semiconducting Oxides, Science 291 (2001)1947-1949.

[3] W. U. Huynh, J. J. Dittmer, A. P. Alivisatos, Hybrid Nanorod-Polymer Solar Cells, Science 295 (2002) 2425-2427.

[4] T. E. Kaiser, H. Wang, V. Stepanenko, F. Würthner, Supramolecular construction of fluorescent J-aggregates based on hydrogen-bonded perylene dyes, Angew Chem. Int. Ed. 46 (2007) 5541-5544

[5] Y. S. Zhao, H. B. Fu, A. D. Peng, Y. Ma, D. B. Xiao, J. N. Yao, Low-dimensional nanomaterials based on small organic molecules: Preparation and optoelectronic properties, Adv. Mater. 20 (2008) 2859-2876.

[6] B. Yang, F.-X. Wang, K.-K. Wang, J.-H. Yan, Y.-Q. Liu, G.-B. Pan, One-step fabrication of

ultralong nanobelts of PI-PTCDI and their optoelectronic properties, Phys. Chem. Chem. Phys.16 (2014) 25251-25254.

[7] C. A. Hunter, K. R. Lawson, J. Perkins, C. J. Urch, Aromatic interactions,J. Chem. Soc., Perkin Trans. 2 (2001) 651-669.

[8] D. Braga, F. Grepioni, How to make weak hydrogen bonds less weak, New J. Chem. 22 (1998) 1159-1161.

[9] C. R. Desiraju, Weak hydrogen bonds in structural Chemistry and Biology, Oxford Univrersity Press, New York, 1990.

[10] P. J. Langley, J. Hulliger, R. Thaimattamb, G. R. Desiraju, Supramolecular synthons mediated by weak hydrogen bonding: forming linear molecular arrays *via* C≡C–H···N≡C and C≡C–H···O_2N recognition, New J. Chem. 22 (1998) 1307-1309.

[11] G. R. Desiraru, R. Parthasarathy, The nature of halogen.cntdot..cntdot..cntdot.halogen interactions: are short halogen contacts due to specific attractive forces or due to close packing of nonspherical atoms?, J. Am. Chem. Soc. 111 (1989) 8725-8726.

[12] J. A. R. P. Sarma, G. R. Desiraju, The Role of Cl···Cl and C-H···O Interactions in the Crystal Engineering of 4-Å Short-Axis Structures, Acc. Chem. Res.19 (1986) 222-228.

[13] C. M. Reddy, M. T. Kirchner, R. C. Gundakaram, K. A. Padmanabhan, G. R. Desiraju, Isostructurality, Polymorphism and Mechanical Properties of Some Hexahalogenated Benzenes: The Nature of Halogen··· Halogen Interactions, Chem. Eur. J.12 (2006) 2222-2234.

[14] A. Mukherjee, S. Tolhadi, G. R. Desiraju, Halogen bonds in crystal engineering: like hydrogen bonds yet different, Acc. Chem. Res. 47 (2014) 2514-2524.

[15] M. Yamamura , S. Ikuma, T. Nabeshima, Herringbone structures of 2,7-dihalogenated acridine tailored by halogen–halogen interactions, J. Mol. Str. 1093 (2015) 59-64.

[16] L. Mei, C.-z. Wang, L. Wang, Y.-l. Zhao, Z.-f. Chai, W.-q. Shi, Halogen Bonded Three-Dimensional Uranyl–Organic Compounds with Unprecedented Halogen–Halogen Interactions and Structure Diversity upon Variation of Halogen Substitution, Crys. Grow. Desg.15 (2015) 1395-1406.

[17] W. H. Ojala, K. M. Lystad, T. L. Deal, J. E. Engebretson, J. M. Spude, B. Balidemaj, C. R. Ojala, Bridge Orientation as a Selector of Intermolecular Interactions in a Series of Crystalline Isomeric Benzylideneanilines, Crys. Grow. Desg. 9 (2009) 964-970.

[18] J.-L. Syssa-Magalé, K. Boubekeur , B. Schöllhorn, First molecular self-assembly of 1,4-diiodo-tetrafluoro-benzene and a ketone via (O···I) non-covalent halogen bonds, J. Mol.

Str.737 (2005) 103-107.

[19] T. Janowski, P. Pulay, High accuracy benchmark calculations on the benzene dimer potential energy surface, Chem. Phys. Lett. 447 (2007) 27-32.

[20] R. A. Distasio Jr., G. v. Helden, R. P. Steele, H.-G. Martin, On the T-shaped structures of the benzene dimer, Chem. Phys. Lett. 437 (2007) 277-283.

[21] E. C. Lee, D. Kim, P. Jurečka, P. Tarakeshwar, P. Hobza, K. S. Kim, Understanding of Assembly Phenomena by Aromatic−Aromatic Interactions: Benzene Dimer and the Substituted Systems, J. Phys. Chem. A 111 (2007) 3446-3457.

[22] M. Pitoňák, P. Neogrády, J. Řezáč, P. Jurečka, M. Urban, P. Hobza, Benzene Dimer: High-Level Wave Function and Density Functional Theory Calculations, J. Chem. Theory Comput. 4 (2008) 1829-1834.

[23] M. O. Sinnokrot, C. D. Sherrill, Substituent Effects in π−π Interactions: Sandwich and T-Shaped Configurations, J. Am. Chem. Soc. 126 (2004) 7690-7697.

[24] M. O. Sinnokrot, C. D. Sherrill, Unexpected Substituent Effects in Face-to-Face π-Stacking Interactions, J. Phys. Chem. A 107 (2003) 8377-8379.

[25] E. G. Hohenstein, C. D. Sherrill, Effects of Heteroatoms on Aromatic π−π Interactions: Benzene−Pyridine and Pyridine Dimer J. Phys. Chem. A 113 (2009) 878-886.

[26] B. K. Mishra, N. Sathyamurthy, STACKING INTERACTION IN PYRAZINE DIMER, J. Theor. Comput. Chem. 5 (2006) 609-620.

[27] S.C. Hartman, J.M. Buchanan, Nucleic acids, purines, pyrimidines (nucleotide synthesis), Annu. Rev. Biochem. 28 (1959) 365-410.

[28] (a) R. Dey, T. Banerjee, V. Langer, S. Ray, P. Roychowdhury, 5-Amino-1-[2-(diethyl amino)ethyl]-1*H*-imidazole-4-carboxamide, Acta. Cryst. E62 (2006) 814-816; (b) R. Dey, T. Banerjee, V. Langer, S. Ray, P. Roychowdhury, 5-Amino-1-benzyl-4-cyano-3-methyl imidazolium toluene-*p*-sulfonate, Acta. Cryst. E61 (2005) 4039-4041; (c) T. Banerjee, S. Chaudhuri, M. Moore, S. Ray, P.S. Chatterjee, P. Roychowdhury, Synthesis and crystal structures of 5-amino-1-(2-hydroxyethyl)imidazole-4-carboxamide and 5-amino-1-(2-chloroethyl)-4-cyanoimidazole, J. Chem. Cryst. 29 (1999) 1281-1286.

[29] S. Ray, A. Das, Studies on the π–π stacking features of imidazole units present in a series of 5-amino-1-alkylimidazole-4-carboxamides, J. Mol. Str. 1089 (2015) 146-152.

[30] M. O. Sinnocort, E. F. Valeev, C. D. Sherrill, Estimates of the Ab Initio Limit for π−π

Interactions: The Benzene Dimer, J. Am. Chem. Soc. 124 (2002) 10887-10893.

[31] X.Wan, H. Zhang, Y. Li, and Y. Chen, Self-assembly based on heterotriangulene derivatives: from nanowiresto microrods, New J. Chem. 34 (2010) 661-666.

[32] *S. Toksoz, H. Acar, M.O. Guker, Self-assembled one-dimensional soft nanostructures*, Soft matter 6 (2010) 5839-5849.

[33] M.J. Frisch, G.W. Trucks, H.B. Schlegel, G.E. Scuseria, M.A. Robb, J.R. Cheeseman, G. Scalmani, V. Barone, B. Mennucci, G.A. Petersson, H. Nakatsuji, M. Caricato, X. Li, H.P. Hratchian, A.F. Izmaylov, J. Bloino, G. Zheng, J.L. Sonnenberg, M. Hada, M. Ehara, K. Toyota, R. Fukuda, J. Hasegawa, M. Ishida, T. Nakajima, Y. Honda, O. Kitao, H. Nakai, T. Vreven, J.A. Montgomery Jr., J.E. Peralta, F. Ogliaro, M. Bearpark, J.J. Heyd, E. Brothers, K.N. Kudin, V.N. Staroverov, R. Kobayashi, J. Normand, K. Raghavachari, A. Rendell, J.C. Burant, S.S. Iyengar, J. Tomasi, M. Cossi, N. Rega, J.M. Millam, M. Klene, J.E. Knox, J.B. Cross, V. Bakken, C. Adamo, J. Jaramillo, R. Gomperts, R.E. Stratmann, O. Yazyev, A.J. Austin, R. Cammi, C. Pomelli, J.W. Ochterski, R.L. Martin, K. Morokuma, V.G. Zakrzewski, G.A. Voth, P. Salvador, J.J. Dannenberg, S. Dapprich, A.D. Daniels, O. Farkas, J.B. Foresman, J.V. Ortiz, J. Cioslowski, D.J. Fox, Gaussian 09, Revision A.02-SMP, Gaussian, Inc., Wallingford, CT, (2009).

[34] G. Chattopadhyay, T. K. Saha, A domino type one-flask synthesis of 1-substituted-5-aminoimidazole-4-carboxamides and ring transformation to pyrazine under microwave through suitable aminoimidazoliumcarboxamide, Ind. J. Chem. 44B (2005) 827-830.

[35] (a) J. P. Colomer, E. L. Moyano, New application of heterocyclic diazonium salts. Synthesis of pyrazolo[3,4-d][1,2,3]triazin-4-ones and imidazo[4,5-d][1,2,3]triazin-4-ones, Tet. Lett. 52 (2011) 1561- 1565;

(b) I. Frank, M. Zeller, 5-Amino-4-Cyano-1-(Hetero)Arylimidazoles, Synth. Comm. 16 (1990) 2519-2526.

[36] P. A. Williams, J. Cosme, A. Ward, H. C. Angove, D. M. Vinkovic´, H. Jhoti, Crystal structure of human cytochrome P450 2C9 with bound warfarin, Nature 424 (2003) 464-468.

[37] G. Kryger, I. Silman, J. L. Sussman, Three-dimensional structure of a complex of E2020 with acetylcholinesterase from *Torpedo californica*, J. Physiol.-Paris 92 (1998) 191-194.

[38] D. F. V. Lewis, M. N. Jacobs, M. Dickins, Compound lipophilicity for substrate binding to human P450s in drug metabolism, Drug discovery Today 9 (2004) 530-537.

[39] W. T. Astbury, F. O. Bell, X-Ray Study of Thymonucleic Acid, Nature (London) 141 (1938) 747-748.

[40] S. L. Cockroft, J. Perkins, C. Zonta, H. Adams, S. E. Spey, C. M. R. Low, J. G. Vinter, K. R. Lawson, C. J. Urchc, C. A. Hunter, Substituent effects on aromatic stacking interactions, Org. Bimol. Chem. 5 (2007) 1062-1080.

[41] M.O. Sinnokrot, C.D. Sherrill, High-Accuracy Quantum Mechanical Studies of π−π Interactions in Benzene Dimers, J. Phys. Chem. A 110 (2006**)** 10656-10668.

[42] S. Tsuzuki, K. Honda, T. Uchimaru, M. Mikami, K. Tanabe, Origin of Attraction and Directionality of the π/π Interaction: Model Chemistry Calculations of Benzene Dimer Interaction, J. Am. Chem. Soc. 124 (2002) 104-112.

[43] K. Reichenbächer, H. I. Süss, J. Hulliger, Fluorine in crystal engineering—"the little atom that could" Chem. Soc. Rev. 34 (2005) 22-30.

[44] M. D. Prasanna, T. N. Guru Row, C-halogen· · π interactions and their influence on molecular conformation and crystal packing: a database study, Cryst. Eng. 3 (2000) 135-154.

[45] S. Terada, K. Katagiri, H. Masu, H. Danjo, Y. Sei, M. Kawahata, M. Tominaga, K. Yamaguchi, I. Azumaya, Polymorphism of Aromatic Sulfonamides with Fluorine Groups, Cryst. Grow. Desgn. 12 (2012) 2908-2916.

[46] F. Cozzi, J. S. Siegel, Interaction between stacked aryl groups in 1,8-diarylnaphthalenes: Dominance of polar/π over charge-transfer effects, Pure Appl. Chem. 67 (1995) 683-689.

[47] S. L. McKay, B. Haptonstall, S. H. Gellman, Beyond the Hydrophobic Effect: Attractions Involving Heteroaromatic Rings in Aqueous Solution[1], J. Am. Chem. Soc. 123 (2001) 1244-1245.

[48] F. Cozzi, R. Annunziata, M. Benaglia, M. Cinquini, L. Raimondi, K. K. Baldridge, J. S. Seigel, Through-space interactions between face-to-face, center-to-edge oriented arenes: importance of polar–π effects, Org. Biomol. Chem.1 (2003) 157-162.

[49] B.W. Gung, X. Xue, H. J. Reich, The Strength of Parallel-Displaced Arene−Arene Interactions in Chloroform J. Org. Chem.70 (2005) 3641-3644.

[50] X. Mei , C. Wolf, Highly Congested Nondistorted Diheteroarylnaphthalenes: Model Compounds for the Investigation of Intramolecular π-Stacking Interactions, J. Org. Chem. 70 (2005) 2299-2305.

[51] M. S. Cubberley, B. L. Iverson, ^{1}H NMR Investigation of Solvent Effects in Aromatic Stacking Interactions, J. Am. Chem. Soc. 123 (2001) 7560-7563.

[52] C. A. Haynam, D. V. Brumbaugh, D. H. Levy, Dimers in jet-cooled s-tetrazine vapor: Structure and electronic spectra, J. Chem. Phys. 79 (1983) 1581-1591.

[53] J. Wanna, J. A. Menapace, E. R. Bernstein, Supersonic molecular jet studies of the pyrazine and pyrimidine dimers, J. Chem. Phys. 85 (1986) 777-784.

[54] B. K. Mishra, N. Sathyamurthy, π−π Interaction in Pyridine, J. Phys. Chem. A 109 (2005) 6-8.

[55] S. Tsuzuki, T. Uchimaru, M. Mikami, K. Tanabe, Basis set effects on the calculated bonding energies of neutral benzene dimers: importance of diffuse polarization functions, Chem. Phys. Lett. 252 (1996) 206-210.

[56] J. E. Galván, D. M. Gil, H. E. Lanús, A. B. Altabef, Theoretical study on the molecular structure and vibrational properties, NBO and HOMO–LUMO analysis of the POX_3 (X = F, Cl, Br, I) series of molecules, J. Mol. Str. 1081 (2015) 536–542.

[57] (a) R.F. Quijano-Quinones, M. Quesadas-Rojas, G. Cuevas, G.J. Mena-Rejón, The Rotational Barrier in Ethane: A Molecular Orbital Study Molecules 17 (2012) 4661-4671;
(b) J. E. Barquera-Lozada, G. Cuevas, Biogenesis of Sesquiterpene Lactones Pseudoguaianolides from Germacranolides: Theoretical Study on the Reaction Mechanism of Terminal Biogenesis of 8-Epiconfertin, J.Org. Chem. 74 (2009) 874-883;
(c) A. Adhikary, A. Kumar, D. Khanduri, M. D. Sevilla, Effect of Base Stacking on the Acid−Base Properties of the Adenine Cation Radical [A•$^+$] in Solution: ESR and DFT Studies, J. Am. Chem. Soc. 130 (2008) 10282-10292.

[58] D. E. Willams, L.-Y. Hsu, Transferability of nonbonded Cl...Cl potential energy function to crystalline chlorine, Acta Cryst. A 41 (1985) 296-301.

[59] G. M. Day, S. L. Price, A Nonempirical Anisotropic Atom−Atom Model Potential for Chlorobenzene Crystals, J. Am. Chem. Soc. 125 (2003)16434-16443.

[60] S. L. Price, A. J. Stone, J. Lucas, R. S. Rowland, A. E. Thornley, The Nature of –Cl.cntdot..cntdot..cntdot.Cl- Intermolecular Interactions, J. Am. Chem. Soc. 116 (1994) 4910-4918.

[61] S. C. Nyburg, W. Wong-Ng, Potential energy interactions in solid dichlorine, Inorg. Chem. 18 (1979) 2790-2791.

[62] S. C. Nyburg, W. Wong-Ng, Anisotropic Atom-Atom Forces and the Space Group of Solid Chlorine, Proc. R. Soc. London Ser. A 367 (1979) 29-45.

[63] F. F. Awwadi, R. D. Willett, K. A. Peterson, B. Twamley, The Nature of Halogen···Halogen Synthons: Crystallographic and Theoretical Studies, Chem. Eur. J.12 (2006) 8952-8960.

[64] Y. S. Zhao, H. Fu, A. Peng, Y. Ma, D. B. Xiao, J. Yao, Low-Dimensional Nanomaterials Based on Small Organic Molecules: Preparation and Optoelectronic Properties, `

[65] (a) J. P. Hill, W. Jin, A. Kosaka, T. Fukushima, H. Ichihara,T. Shimomura, K. Ito, T. Hashizume, N. Ishii, T. Aida, Self-Assembled Hexa-peri-hexabenzocoronene Graphitic Nanotube, Science 304 (2004) 1481-1483; (b) H. Liu, Y. Li, S. Xiao, H. Gan, T. Jiu, H. Li, L. Jiang, D. Zhu, D. Yu, B. Xiang,Y. Chen, Synthesis of Organic One-Dimensional Nanomaterials by Solid-Phase Reaction, J. Am. Chem. Soc. 125 (2003) 10794-10795; (c) H. Liu, Y. Li, L. Jiang, H. Luo, S. Xiao, H. Fang, H. Li, D. Zhu, D. Yu, J. Xu , B. Xiang, Imaging As-Grown [60]Fullerene Nanotubes by Template Technique, J. Am. Chem.Soc. 124 (2002) 13370-13371.

[66] (a) T. E. Kaiser, H. Wang, V. Stepanenko, F. Würthner, Supramolecular Construction of Fluorescent J-Aggregates Based on Hydrogen-Bonded Perylene Dyes, Angew. Chem. Int. Ed. 46 (2007) 5541-5544; (b) T. Naddo, Y. K. Che, W. Zhang, K. Balakrishnan, X. M. Yang,M. Yen, J. C. Zhao, J. S. Moore, L. Zang, Detection of Explosives with a Fluorescent Nanofibril Film, J. Am. Chem. Soc. 129 (2007) 6978-6979; (c) A. Ajayaghosh, S. J. George , A. P. H. J. Schenning, Hydrogen-bonded assemblies of dyes and extended π-conjugated systems Top. Curr. Chem. 258 (2005) 83-118.

[67] A. Xie, F. Wu, W. Jiang, K. Zhang, M. Sun, M. Wang, Chiral induced synthesis of helical polypyrrole (PPy) nano-structures: a lightweight and high-performance material against electromagnetic pollution, J. Mater. Chem. C 5 (2017) 2175-2181.

[68] W. U. Huynh, J. J. Dittmer, A. P. Alivisatos, Hybrid Nanorod-Polymer Solar Cells, Science 295 (2002) 2425-2427.

[69] Z. W. Pan, Z. R. Dai , Z. L. Wang, Nanobelts of Semiconducting Oxides, Science 291 (2001) 1947-1949.

[70] K. Balakrishnan, A. Datar, R. Oitker, H. Chen, J. M. Zuo , L. Zang, Nanobelt Self-Assembly from an Organic n-Type Semiconductor: Propoxyethyl-PTCDI, J. Am. Chem. Soc. 127 (2005) 10496-10497.

- Synthesis of 1-(phenyl/*p*-halophenyl)AICA and its nitrile derivatives.
- Study the change in stacking patterns with functional group change.
- Role of halogens for fixing the stacking patterns.
- DFT study to quantify T-stacking and π-π stacking of imi-imi and phe-phe.
- Investigation of nano-structural behavior.